Synthesis and Study of Structural and Vibrational Spectral Contributions to the Nonlinear Optical Properties of (2E)-2-(3,4-Dimethoxybenzylidene)-3,4-dihydronaphthalen-1(2H)-one

Dissertation submitted to

The University of Kerala

In partial fulfilment of the requirements for the award of the degree of

MASTER OF SCIENCE IN PHYSICS

2020-2022

ABSTRACT

The chalcone derivative (2E)-2-(3,4-Dimethoxybenzylidene)-3,4-dihydronaphthalen-1(2H)-one was synthesized and single crystals were grown by slow evaporation technique. Its structure was examined by X-ray diffraction analysis and investigated theoretically as well as experimentally to examine its nonlinear optical (NLO) behaviour. Density Functional Theory was used to obtain the theoretical calculations using Gaussian 09W program package. Cc-pVTZ level of theory was used to obtain the geometry optimization of the title compound. The calculated optimized parameters were tabulated. The vibrational spectral analysis of the compound have been carried out using the experimental and computational FT-IR evaluation. The theoretical and experimental cut off wavelength, corresponding to electronic transitions are obtained. The most important hyper conjugative interactions leading to the stability and intramolecular charge transfer of the compound is sort out by natural bond orbital analysis. The active frontier molecular orbitals play a part in the electronic transitions were identified. The nonlinear optical behaviour was investigated theoretically and third order nonlinearity of (2E)-2-(3,4-Dimethoxybenzylidene)-3,4-dihydronaphthalen-1(2H)-one crystal, measured from z-scan studies, conducted in continuous wave excitation regime was also done.

CONTENTS

CHAPTER 1

INTRODUCTION

1.1.GENERAL INTRODUCTION TO RESEARCH WORK AND MOTIVATION

Chalcones are a group of plant-derived polyphenolic compounds belonging to the flavonoid family. They are α, β-unsaturated ketones- 1,3-diphenyl-2-propene-1-one. A variety of important biological compounds are known collectively as chalcones or chalconoids.

Chalcones and its derivatives have become the material of attraction in the past few decades due to their availability in natural products, structural flexibility, biological activities and high optical nonlinearities that they can exhibit due to the significant delocalisation of the electronic clouds. Also, they possess a broad spectrum of various properties because of which they are among the most active research objects in science, nowadays. Chalcone is one of the most privileged scaffolds in medicinal chemistry that can be synthesized in the laboratory and that can be converted into several therapeutically active heterocyclic scaffolds. It exhibits pharmacological activities and also plays a key role in several non-pharmacological applications. Chalcones and its synthetic derivatives are well known to possess antimicrobial, antioxidant, anti-inflammatory, anticancer, anti-histaminic, anti-protozoa, hypnotic effects, and other significant activities depending on the substitution made on them [1].

The discovery of new crystals for optical applications has been an emerging area of research, along with the increased studies on the optical properties of materials. Both organic and inorganic materials are studied extensively. Crystals with the nonlinear optical response (NLO) are significant in science and modern technology because of their technological importance in the areas of optical communication, optical modulators, optical switching, information processing, frequency conversion and doubling, data storage etc. and are expected to play an important role in facilitating optoelectronic and photonic developments. Usually, organic materials show excellent NLO properties and hence the growth of new organic-based single crystal is important [2].

The chalcone derivatives have attracted significant attention because of their molecular structure and synthetic flexibility that can modify their NLO properties. These properties are reflected by the

significant delocalization of π electrons of the chalcone system. The chalcone derivatives with a π conjugated system represent an ideal NLO system, as there is a possibility of large charge transfer through substituent groups on aromatic rings. The interest for novel chalcone-based materials in nonlinear optics is dependent on strong second harmonic generation in organic systems. High crystallinity exhibited by chalcones also add their applications in second and third order NLO. Along with these properties, thermal stability, good optical limiting behaviour are also advantageous for its applications [3,4].

The quantum mechanical investigations on the structure, electronic and vibrational spectra of an organic chalcone derivative -(2E)-2-(3,4-Dimethoxybenzylidene)-3,4-dihydronaphthalen-1(2H)-one is expected to be done in this project. Computational quantum chemistry, which uses many approximation methods, including Density functional theory is used in this work to obtain necessary information about the many-electron system under study.

Computer simulations which act as a connecting link between analytic theory and experiment, allowing to scrutinize theories, can also be used as an explanatory research tool under physical conditions not feasible in real laboratory experiments. Thus, a new interdisciplinary research approach- Computational Material Science or Computational Physics- was established, which brings together elements from diverse fields of study such as Physics, Chemistry, Mathematics, Biology, Engineering and even Medicine. Multiscale and multidisciplinary simulations in realistic situations can also be done with this method. It can be used to determine the structure and properties of molecules. Computational results normally complement the information obtained from experimental results. However, in some cases it can predict hitherto unobserved chemical phenomena. The information about the system (molecule/group of molecules/solids) derived by this method includes structure, absolute and relative (interaction) energies, vibrational frequencies, reactivity, electronic charge density, other spectroscopic quantities etc.

In quantum chemical methods, the basics is to obtain the approximate solutions of the Schrödinger equation corresponding to the many-electron system, and several methods in the domain of quantum physics have been developed and implemented in computational programs for this. Ab initio methods, density-functional methods, semi-empirical methods are some of the methods used by such programs. The majority of chemical phenomena can be described to a certain degree in a qualitative or approximate quantitative computational scheme.

CHAPTER 2

THEORETICAL BACKGROUND

2.1 QUANTUM CHEMICAL CALCULATIONS

A field of Chemistry that uses mathematical approximations and computer programs to solve problems of chemical interest is called Computational chemistry, and Quantum chemistry is its subfield that addresses the equations and approximations derived from the postulates of quantum mechanics which specifically involves solving the Schrödinger equation for molecular systems. The role of Quantum chemical calculations in chemical research and teaching is ever-increasing. It was the introduction of Quantum Mechanics which provided various methods to obtain information about quantum systems, by making the use of Mathematics common.

Every Quantum problem aims at solving the Schrödinger equation corresponding to the system under study. Because of its complexity, it is not so simple to solve the equations of complex systems analytically. Hence to solve it, different approximation methods need to be applied. For very accurate results, these methods are performed multiple times. This is very difficult and tedious to do by hand, so the role of computers comes into play. With the advancement in computer technology, a good deal of software that makes use of different quantum approximation methods were developed. Along with its easy availability, this made much contribution to the research fields, especially in physics and chemistry, where computations have so much importance. The system under study may be a molecule, a group of molecules, or a solid. Computational chemistry calculations use very approximate and accurate (only for small systems) calculations. The two important methods widely used are the following:

2.1.1 Ab-initio Methods

The fundamental aim of quantum chemical computations, as already said above, is to solve the Schrödinger equation and to find an approximate solution for the corresponding system. Among the various methods implemented to do this, the Ab-initio methods are based on theoretical principles and universal physical constants without involving experimental data. The term Ab-initio, meaning “from first principles” or “from the beginning” itself implies that the only inputs into an ab-initio calculation

are physical constants. These strategies are exceptionally thorough scientific approximations. These methods extend from the first-principles equations in their simplified form, which are very easier or faster to solve to approximations limiting the size of the system (for example, periodic boundary conditions), to basic approximations to the fundamental conditions that compare to the system. Hartree-Fock method, configuration interaction Moller-Plesset perturbation theory, coupled-cluster and reduced density matrices are some categories of ab-initio methods that are widely used in quantum chemistry and physics. Given the positions of the nuclei and the number of electrons, these quantum chemical methods look for approximate solutions to the electronic Schrödinger equation, in order to yield useful information such as electron densities, energies and other properties of the system under study. Thus, based on the laws of quantum mechanics, Ab-initio methods allow the determination of the fundamental properties of materials.

Empirical or semi-empirical methods uses additional empirical parameters, as the name suggests. Parameters derived from experimental data are used in these methods to simplify the calculations. These methods provide a substantial reduction in the required computation time and, consequently, the ability to execute calculations for large molecules is high. Hence these methods are often applied to large systems. These strategies are generally cheap and can give a reasonably qualitative description of molecular systems and decently exact quantitative forecasts of energies and structures for frameworks where good parameter sets exist. On the other hand, the computations in Ab initio methods are completely based on the fundamental laws of quantum mechanics. Without using any experimental parameters, they are able to supply high-quality quantitative forecasts for a wide range of systems and are not constrained to any particular class or measure of a system.

Consider a polyatomic system -an isolated molecule or the atoms defining the crystal of any particular mineral of interest. A vital perception in applying quantum mechanics to molecules is that nuclear cores are much heavier than individual electrons. The primary step within the calculation is to solve equations corresponding to the electron motion, for fixed positions of the atomic nuclei. For a given set of electrons moving within the field of a set of cores, we discover the configuration with the lowest energy, or state, of the electrons. This lowest energy state is called the ground state of the electrons and the separation of the nuclei and electrons into separate mathematical problems is the Born-Oppenheimer approximation. The calculations in quantum mechanical method involve solving the time-independent Schrödinger equation given by,

$$H\psi = E\psi \qquad (1)$$

Where H is the Hamiltonian of the system and ψ, the total wave function of the system. The circumstance we are inquisitive about where different electrons are association with numerous cores is more complicated. Here, the complete Schrödinger equation is:

$$\left[-\frac{h^2}{2m} \sum_{i\ 1}^{N} \nabla_i^2 + \sum_{i\ 1}^{N} V(\mathbf{r}_i) + \sum_{i\ 1}^{N} \sum_{j<i} U(\mathbf{r}_i, \mathbf{r}_j) \right] \psi = E\psi. \qquad (2)$$

Where m is the mass of the electron. The first, second and the third term (inside the bracket) define the kinetic energy of each electron, the interaction energy between each electron and the collection of atomic nuclei, and the interaction energy between different electrons respectively. Since the electronic wave function is a function of each of the spatial coordinates of each of the N electrons, $\psi=\psi(r_1,r_2,\ldots,r_N)$, and E is the ground state energy of the electrons. It is possible to write the electron wave function, which is a function of each of the coordinates of the N electrons, as the product of each of the individual wave functions. The expression for this wave function which is called the Hartree product is $\Psi=\psi_1(r_1)\psi_2(r_2)\ldots\psi_N(r_N)$. That is, the wave function of a many-particle system is obtained as a combination of single particle wave functions, as given by the Hartree product. Its basis is the independent particle model, where each particle is expected to be in a mean-field resulting from all the other electrons and nuclei. This method didn't respect the principle of anti-symmetry of the wave function and hence doesn't take into consideration the idea of Pauli's exclusion principle.

In electron coordinates, the Hartree total wave function of an atom is not antisymmetric. A generalized method considering the antisymmetric nature of wave function was put forward by V. A. Fock and J. C. Slater in 1930, and is known as Hartree-Fock method. The Hartree-Fock (HF) method is a method of approximation for the determination of the wave function and the energy of a quantum many-body system in a stationary state. As there are no known analytic solutions for many-electron systems, numerical methods are used. For solving the equations, non-linear method such as iteration come into play since nonlinearities are introduced by the Hartree-Fock approximation and hence, this method is also known as the Self Consistent Field method (SCF). In this approach, the N-electron wave function is assumed to be a Slater determinant. That is, the wave function is an antisymmetric product of individual electron-spin orbitals. This assumption was made in accordance with the single particle model and the Pauli's exclusion principle. The slater determinant is then optimized by variational method, to find the best individual electron spin-orbitals. Thus, for a many-electron system, the SCF method can be called a particular case of the variational method, with its trial wave function a slater determinant. In the determination of atomic wave functions and energies, this method can be considered

as the first step as the many-electron wave function solution of the Schrödinger equation can only be represented as the infinite sum of slater determinants. The Hartree-Fock method finds its typical application in the solution of the Schrödinger equation for molecules, nanostructures and solids along with that of atoms.

The Hartree-Fock energy is the minimal energy for a single slater determinant and the starting point for this method is a set of exact one-electron wave functions known as spin-orbitals.

In Hartree-Fock theory the wave function of a many-electron system, represented by the Slater determinant has the form

$$\Phi(q_1, q_2, \ldots q_N) = \frac{1}{\sqrt{N!}} \begin{vmatrix} u_\alpha(q_1) & u_\beta(q_1) \cdots & u_\nu(q_1) \\ u_\alpha(q_2) & u_\beta(q_2) \cdots & u_\nu(q_2) \\ \vdots & & \\ u_\alpha(q_N) & u_\beta(q_N) \cdots & u_\nu(q_N) \end{vmatrix} \tag{3}$$

Where α, β,……,ν denotes a set of four quantum numbers (n, l, m_l, m_s). From this determinant, it is clear that if two or more sets of individual quantum numbers α, β, …, ν are equal, the determinant vanishes and hence, the wave function also vanishes. That is, only one fermion can occupy a given quantum state -The Pauli's exclusion principle.

Using the variational principle, the ground state energy is:

$$E_0 \leqslant E[\Phi] = \langle \Phi | H | \Phi \rangle \tag{4}$$

Where φ is normalized to unity.

The Spin orbitals u_α, u_β,….., u_ν are found out from the set of integro-differential equations,

$$\left[-\frac{1}{2} \nabla_{r_i}^2 - \frac{Z}{r_i} \right] u_\lambda(q_i) + \left[\sum_\mu \int u_\mu^\star(q_j) \frac{1}{r_{ij}} u_\mu(q_j) \, dq_j \right] u_\lambda(q_i) - \sum_\mu \left[\int u_\mu^\star(q_j) \frac{1}{r_{ij}} u_\lambda(q_j) \, dq_j \right] u_\mu(q_i) = E_\lambda u_\lambda(q_i)$$
$$\lambda, \mu = \alpha, \beta, \ldots \nu \tag{5}$$

such that the function E(φ) is minimum. The above set of equations are known as the Hartree-Fock equations and the orbitals are termed as Hartree-Fock orbitals.

As already said, Hartree-Fock equations are solved iteratively. Firstly, the Hartree-Fock potential $V^{(1)}$ is calculated from the approximate spin orbitals $u_\alpha^{(1)}$, $u_\beta^{(1)}$,….., $u_\nu^{(1)}$. Then by solving the set of orbitals for this potential, a new set of spin orbitals $u_\alpha^{(2)}$, $u_\beta^{(2)}$,….,$u_\nu^{(2)}$ is obtained. These steps are repeated n times until the final set of orbitals whose potential $V^{(n)}$ is identical (within the desired approximation) to the potential $V^{(n-1)}$ calculated in the previous iteration step. This potential field is known as the self-consistent field of the particular system. Be that as may, Hartree-Fock orbitals are not exact orbitals, they can only be a beginning point for more refined calculations [5,6,7].

The algorithmic flowchart illustrating the Hartree-Fock method is shown below:

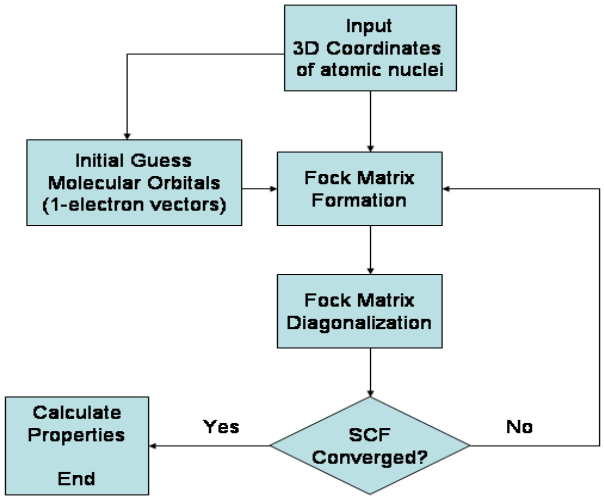

Thus, in Hartree-Fock method, along with the use of Born-Oppenheimer approximation, the relativistic effects are neglected, the variational solution is assumed to be a linear combination of a finite number of orthogonal (usually, but not always) basis functions while the energy eigen function is seen to be described by a single slater determinant. But for calculations in this method, the correlation between the electrons of anti-parallel spins is neglected. The correlation energy is the difference between the Hartree-Fock energy and the exact energy and hence, its neglectance results in large deviations from the experimental results. On using ab-initio methods, the incomplete treatment of electron correlation, deviations from the Born-Oppenheimer approximation, incompleteness of basis sets, and neglect of relativistic effects (for heavy atomic molecules) are the seeds of error in molecular electronic calculations. Among them, the basis set and electron correlation effects are the important error-sources. Taking consideration of this, a number of approaches have been devised to include electron correlation to the multi-electron wave function, and they are collectively called post-Hartree-Fock methods.

A new set of electronic structure methods, called Density Functional methods are similar to ab-initio methods in many ways and can be used as an alternative to Hartree-Fock (HF) calculations in some cases as it requires about the same amount of computation resources as the least expensive Hartree-Fock theory. The Density Functional Theory (DFT) treats both exchange and correlation energies, though approximately. The electron correlation is that the electrons in a molecular system react to one another's motion and try to keep out of one another's way. The HF method is an exchange only method as it considers the correlation in an average sense. In HF method, it is assumed that each electron sees and reacts to an averaged electron density. There are no HF methods with electron correlations to account for the instantaneous interactions of electron pairs with opposite spin. Due to this, the accuracy of HF results cannot be assured in some types of systems. Thus, at the Hartree-Fock cost, the benefits of some more expensive ab-initio methods can be obtained by using DFT methods.

2.1.2 Density Functional Theory

Density Functional Theory (DFT) is a computational quantum mechanical modelling method used to study the electronic structure of many-body systems, especially atoms, molecules, and the condensed phases, in physics, chemistry and material science. In this theory, functionals, i.e., the functions of another function, is used to determine the properties of a many-electron system. These are functionals of electron density. Along with its advantages like the consideration of correlation, low cost compared to the traditional methods (viz. HF method), the accuracy and efficiency offered by it is especially important for large systems.

Hohenberg-Kohn theorems

The density functional theory has its foundation on two fundamental theorems proved by Kohn and Hohenberg and a set of equations derived by Kohn and Sham.

Theorem 1: *The ground state energy from Schrödinger's equation is a unique functional of the electron density.*

According to this theorem, there exists a one-to-one mapping between the ground-state wave function and the ground-state electron density. Hence by this, the ground-state energy E can be expressed as a function of electron density n(r), i.e., E[n(r)]. This is why this field is known as density functional theory. Hohenberg and Kohn's result can also be restated as: the ground-state electron density uniquely determines all properties, including the energy and wave function, of the ground state.

Even though the theorem rigorously proves that a functional of the electron density exists that can be used to solve the Schrödinger equation, it says nothing about what the functional actually is. An important property of the functional is given by the second Hohenberg-Kohn theorem [8].

Theorem 2: *The electron density that minimizes the energy of the overall functional is the true electron density corresponding to the full solution of the Schrödinger equation.*

If the appropriate functional form is known, the electron density can be varied until the energy from the functional is minimized, which can give some information for finding the relevant electron density. This variational principle is used in practice with approximate forms of the functional.
The functional described by the Hohenberg-Kohn theorem is in terms of the single-electron wave functions, $\psi_i(r)$. These functions collectively define the electron density n(r). The energy functional can be written as:

$$E[\{\psi_i\}] = E_{\text{known}}[\{\psi_i\}] + E_{\text{XC}}[\{\psi_i\}], \tag{6}$$

Here the functional is split into a collection of terms which can be written in a simple analytical form, $E_{known}[\{\psi_i\}]$, and everything else, E_{XC}. The "known" terms include four contributions:

$$E_{\text{known}}[\{\psi_i\}] = -\frac{\hbar^2}{2m}\sum_i \int \psi_i^* \nabla^2 \psi_i d^3r + \int V(\mathbf{r}) n(\mathbf{r})\, d^3r + \frac{e^2}{2}\int\int \frac{n(\mathbf{r})n(\mathbf{r}')}{|\mathbf{r}-\mathbf{r}'|}\, d^3r\, d^3r' + E_{\text{ion}}. \tag{7}$$

The first, second, third and the fourth terms on RHS are the electron kinetic energies, the Coulomb interactions between the electrons and the nuclei, the Coulomb interactions between pairs of electrons, and the Coulomb interactions between pairs of nuclei respectively.

The term $E_{XC}[\{\psi_i\}]$ is the *exchange-correlation functional* and is defined such that it includes all the quantum mechanical effects that are not included in the "known" terms.

Kohn and Sham showed that the task of finding the right electron density can be expressed in a way that involve solving a set of equations in which each equation only involves a single electron. The Kohn–Sham equations have the form,

$$\left[-\frac{\hbar^2}{2m}\nabla^2 + V(\mathbf{r}) + V_H(\mathbf{r}) + V_{\text{XC}}(\mathbf{r})\right]\psi_i(\mathbf{r}) = \varepsilon_i \psi_i(\mathbf{r}). \tag{8}$$

The solution of the Kohn–Sham equations are single-electron wave functions that depend on only three spatial variables, $\psi_i(r)$. There are three potentials, V , V_H , and V_{XC}, on the left − hand side of the Kohn− Sham equations.The first potential is the same as appeared in Schrödinger equation. This potential defines the interaction between an electron and the collection of atomic nuclei. The second is called the Hartree potential and is defined by:

$$V_H(\mathbf{r}) = e^2 \int \frac{n(\mathbf{r}')}{|\mathbf{r} - \mathbf{r}'|} d^3 r' \tag{9}$$

The above potential describes the Coulomb repulsion between the electron being considered in one of the Kohn–Sham equations and the total electron density defined by all electrons in the problem. Since the electron we are describing in the Kohn–Sham equation is also part of the total electron density, the Hartree potential includes a so-called self-interaction contribution. So, part of V_H involves a Coulomb interaction between the electron and itself. The self-interaction is unphysical, and the correction for it is one of several effects that are combined together into the final potential in the Kohn–Sham equations, V_{XC}, which defines exchange and correlation contributions to the single electron equations. V_{XC} can formally be defined as a "*functional derivative*" of the exchange–correlation energy:

$$V_{\mathrm{XC}}(\mathbf{r}) = \frac{\delta E_{\mathrm{XC}}(\mathbf{r})}{\delta n(\mathbf{r})}. \tag{10}$$

The functional derivative is written using δ rather than d to emphasize that it not quite identical to a normal derivative. The problem of solving the Kohn-Sham equations is usually treated in an iterative way as outlined in the following algorithm:

1. Define an initial, trial electron density, $n(r)$
2. Solve the Kohn–Sham equations defined using the trial electron density to find the single-particle wave functions, $\psi_i(r)$.
3. Calculate the electron density defined by the Kohn–Sham single particle wave functions from step 2, $n_{KS} = 2\sum_i \psi_i^*(r)\psi_i(r)$.
4. Compare the calculated electron density, n_{KS}, with the electron density used in solving the Kohn–Sham equations, $n(r)$. If the two densities are the same, then this is the ground-state electron density, and it can be used to compute the total energy. If the two densities are different, then the trial electron density must be updated in some way. Once this is done, the process begins again from step 2 [8].

Basis Sets

The introduction of a basis set is one of the important approximations associated with essentially all ab-initio methods. In theoretical and computational chemistry, the basis set can be seen as a set of functions called the basis functions. It is a mathematical description of the orbitals within a system which is used to carry out different theoretical calculations about the system under study, since the molecular orbitals used for quantum chemical calculations can be obtained by combining the basis sets in a linear combination. To make the equations appropriate for effective usage in a computer, the basis sets are used for representing the electronic wave function in DFT or Hartree-Fock method. For simplicity, these functions are considered as atomic orbitals centred on atoms (normally used in quantum chemical calculations), but theoretically it can be any function, like plane waves (used frequently in the field of solid-state physics). A finite set of basis functions are used in modern computational chemistry, to perform calculations based on quantum chemistry and physics. When the finite basis is expanded towards an(infinite) complete set of functions, calculations employing such a basis set are said to approach the complete basis set (CBS) limit. Such basis functions are centred on the atoms and are sometimes referred to as Atomic Orbitals(AO),even if they are not solutions to an atomic Schrodinger equation in general. Each electron can be viewed to be limited to a particular region of space due to the basis set. Smaller basis sets impose more constrains on the electrons, while larger ones cause fewer restrictions and approximate each orbital more accurately. But larger basis sets require more computational resources. Mathematically, the molecular wave function can be approximated as the linear combination of the atomic orbitals (basis functions),as:

$$\phi_i = \sum_{k=1}^{n} C_{ki}\chi_i \qquad (11)$$

where ϕ_i is the i^{th} molecular orbital, C_{ki} are the coefficients of linear combination. The basis functions $\chi_1,\chi_2,\ldots\ldots,\chi_n$ are chosen to be normalized [8,9,10].

Slater and Gaussian Type Orbitals

In electronic structure calculations, there are two commonly used basis functions: Slater Type Orbitals (STO) and Gaussian Type Orbitals (GTO). The Slater Type Orbitals have the functional form:

$$\chi_{\zeta.n.l.m}(r,\theta,\varphi) = NY_{l.m}(\theta,\varphi)r^{n-1}e^{-\zeta r} \qquad (12)$$

Where, N is a normalization constant and $Y_{l.m}$ are spherical harmonic functions. For hydrogen-like atoms, it can be seen that the exponential dependence on the distance between the nucleus and electron is similar to that of the exact orbitals for hydrogen-like atoms.[9]

To be more exact, a double zeta basis may be used for molecular orbital calculations and has the form:

$$\chi \propto r^{n-1}\left[c_1 e^{-\zeta_1 r} + c_2 e^{-\zeta_2 r}\right]Y \qquad (13)$$

where now the atomic energy is minimized with respect to ζ_1 and ζ_2.[9, 10]

Gaussian-Type Orbitals (GTOs) can be written in terms of Cartesian coordinates as:

$$\chi(x,y,z) \propto x^i y^j z^k e^{-\propto r^2} \qquad (14)$$

where i, j, k are positive integers or zero. $\propto$ in the exponential is the orbital constant. The sum of i, j, k determines the type of orbital. (i.e., orbitals of s, p and d type results when i + j + k = 0,1,2 respectively). [9, 10]

The great convenience of GTOs is that the evaluation of the molecular integrals needed in ab initio calculations is done much more efficiently. In practice the functional behaviour of STOs is found by combining a number of GTOs with different orbital exponents [10].

$$e^{-\zeta r} \approx c_1 e^{-\propto_1 r^2} + c_2\, e^{-\propto_2 r^2} + \cdots \qquad (15)$$

where GTOs with large and small exponents are designed to fit the centre and tail portions, respectively, of an STO. The GTOs used here are called primitive Gaussian functions, while their linear combinations are called contracted Gaussian basis function. The atomic wave functions are said to be of STO-nG quality, if n GTOs are used to fit each STO [10].

A minimum or Single Zeta (SZ) basis set is the set of smallest number of functions possible where, only enough functions are employed to contain all the electrons of the neutral atom(s). For Hydrogen (and Helium), this is a single s-function. For the first row in the periodic table, it is two s-functions (1s & 2s) and one set of p-functions ($2p_x$, $2p_y$, $2p_z$). For the second-row elements, a minimum basis set has three s-functions (1s, 2s & 3s) and two sets of p-functions (2p and 3p) are used.

To get more accurate results the basis sets can be improved by doubling all the basis functions, producing a Double Zeta (DZ) type basis. The term zeta is from the fact that the exponent of STO basis functions is often denoted by the Greek letter ζ. For hydrogen, a *DZ* basis set use two s-functions (1s and 1s′). This basis set employs four s-functions(1s, 1s′, 2s and 2s′) and two p-functions(2p and 2p′) for first row elements. For second row elements, DZ basis consists of six s-functions and four p-

functions. Doubling the number of basis functions allows for a much better description of the fact that the electron distribution is different in different directions. In similar way ***Triple Zeta* (*TZ***) basis is also used where the basis function contains three times as many functions as the SZ basis [10].
The split valence basis set is a variation in DZ basis set in which only the no: of valence orbitals is doubled. An example is:

$$H: 1s, 1s\ '$$

$$C: 1s\ ,2s, 2s\ ', 2p_x\ ,2p_y\ ,2p_z\ ,2p_x', 2p_y', 2p_z'$$

Here the primed and unprimed orbitals have different sizes.

The use of such minimum basis sets put a restriction on the variation that can be made on the electronic charge, to describe molecules and chemical bonds, from the free electronic charge distribution in the free atom case. A relaxation in this can be obtained by including higher angular momentum orbitals in addition to that required for the description of ground state of each atom. Such functions are called "polarization" function and the corresponding basis set is called **Polarization basis set**. This can be used for the best reproduce of the observables like molecular geometry. For modelling chemical bonding, where the bonds are often polarized, the polarization basis set is very important. The addition of d-functions to carbon atoms (which has basis set with p-valence orbitals) and that of p-functions to hydrogen atoms (which has basis set with s-valence orbitals) by the polarized basis set are some of its examples. By the use of variational method, the polarization functions will lower the total energy calculated for the molecule. Also, the use of such functions will result in better matching of observed and calculated geometries.

The basis sets can be further modified by the addition of **diffuse functions**-large size versions of s- and p- type functions. Such functions can be viewed as the extended Gaussian basis functions with a small exponent. These allow the orbitals to occupy a larger region of space, by providing flexibility to the "tail" portion of the atomic orbitals, far away from the nucleus. Thus, for systems where electrons may occupy far from the nucleus, the basis sets involving diffuse functions are important [9,11].

2.2 GEOMETRY OPTIMIZATION

Geometry optimization is very important step in the computational chemistry studies that are focussed on the structure and/or reactivity of molecules. The structure of a molecule can be pointed out by providing the atomic locations in the molecule. A molecule has a specific energy for a given structure and electronic state. The variation of the energy of the molecule in a particular state as a function of the structure of the molecule is given by a Potential energy surface. The Potential Energy Surface (PES)

which is a central concept in computational chemistry, has very much importance in the analysis of molecular geometry and chemical reaction dynamics. It is because, they help us to visualize and understand the relationship between the potential energy and the molecular geometry, and to understand how computational chemistry programs locate and characterize structures of interest. The minimum and the saddle points are the important points of interest and are called stationary points. The first derivative of the energy vanishes at these points. Since the negative of the gradient is the vector of forces on the atoms in the molecule, the forces are also zero at these points. Thus, stationary points are points on the potential energy surface where the forces are zero [11,12].

A simple representation of a potential energy surface (PES) is given in the figure below:

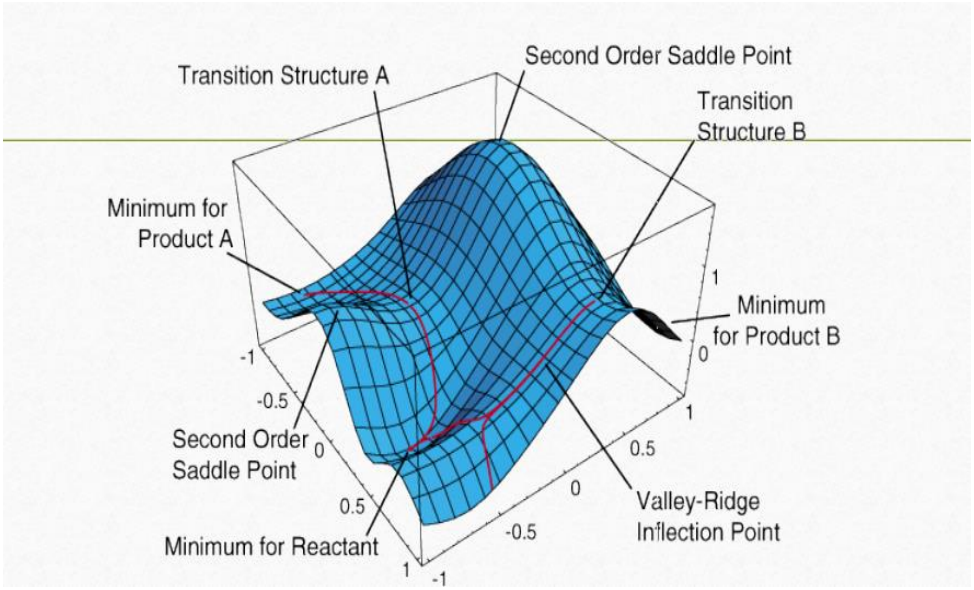

Figure 2.2.1: Features of Potential Energy Surface

Regarding computational chemistry, Geometry optimization (also called energy optimization or energy minimization) is the process of finding an arrangement of a collection of atoms in space such that the net inter-atomic force on individual atom is close to zero and the position on the potential energy surface (PES) is a stationary point. A single molecule, an ion, a condensed phase, a transition state or even a collection of any of these may be regarded as the collection of atoms. Usually, the potential energy surface may have more than one Local Minima and one Global Minima (lowest energy points in PES) [11].

The geometry optimization process involves the calculation of the wave function and the energy at a starting geometry and then proceeding to find a new geometry of a lower energy. The iteration goes on until the lowest energy geometry is obtained. The first derivative (or gradient) with respect to atomic

positions is evaluated to find the force on each atom. Then for a rapid convergence to the lowest energy geometry, refined algorithms are used to select a new geometry, at each step. The result converges to the final minimum energy geometry for which the force on each atom is zero, at one point .It should be noted that this procedure does not guarantees the lowest energy geometry as a result (global minimum in the PES diagram) always.

Frequency Calculation

The nuclei in molecules are in continuous motion in the practical case. At equilibrium states, these vibrations are regular and hence, predictable. Then the molecule can be identified because of their characteristic spectra. The vibrational spectra of the molecules in their ground and excited states can be computed by the Chemical computation software. The program can predict the frequencies and intensities of spectral lines, and also it can describe the normal mode vibrations executed by the system. The program also predicts the direction and magnitude of the nuclear displacement occurring in the system on absorbing a quantum of energy. The frequency calculations must be done on optimized structures, since the frequency calculations are valid only at stationary points on the PES.

2.3 NATURAL BOND ORBITAL (NBO) ANALYSIS

One of the methods for translating the computational results of Schrodinger's wave equation into the familiar language of chemical bonding concepts is the Natural bond orbital (NBO) analysis. These methods involve a set of mathematical algorithms to analyse electronic wave functions in the localized Lewis-like chemical bond language. The molecular properties are described in terms of a 'natural Lewis structure' depiction of the wave function, in direct reference to the elementary Lewis dot diagram in chemistry, in such methods.

In natural bond analysis, a series of transformations from the input basis set to various localized basis sets such as natural atomic orbitals (NAOs), natural hybrid orbitals (NHOs), natural bond orbitals (NBOs), and localized molecular orbitals (NLMOs) are involved:

Input basis→ NAOs→ NHOs→ NBOs→ NLMOs→ Molecular orbitals

Then, the localized sets may be converted to delocalized natural orbitals (NOs) or canonical molecular orbitals (MOs). NBOs are formulated in terms of a complete orthonormal set which describe the effective atom-like constituents within the molecular environment optimally, called the natural atomic orbitals (NAOs) $\{\theta_i^{(A)}\}$.The NAOs normally converges to the corresponding atomic natural orbitals of

isolated atoms under large interatomic separation limits. The NAOs shows size and shape variations, and are distinguished clearly from free atom forms in a given molecular system.

The natural bond orbitals (NBOs) are one-centred or two-centred (or more) localized orbitals that give a Lewis-type description of the chemical bond. Each one-center (1c) lone pair or two-center(2c) bond pair of the Lewis structure diagram is related with a 'Lewis' (L type) member of the complete orthonormal set of NBOs ,where the completion of span of the basis and the description of residual resonance delocalization effects (departure from the idealized L-type representation) are done by the remaining 'non-Lewis' (NL type) NBOs .

Lewis-type NBO Ω_{AB} can be written in terms of two directed valence hybrids(NHOs) h_A and h_B on atoms A and B, with corresponding polarization coefficients c_A and c_B as:

$$\Omega_{AB} = c_A h_A + c_B h_B \qquad (16)$$

Where c_A and c_B satisfy $|c_A|^2 + |c_B|^2 = 1$. Depending on the coefficient values, the NBO character can vary smoothly between covalent ($c_A = c_B$) or ionic ($c_A \gg c_B$) limit. Such natural localized functions has a characteristic feature that is the simultaneous requirement of ***orthonormality*** and ***maximum occupancy,*** which ***leads*** to compact expressions for atomic and bond properties.
The NHOs are optimized linear combination of valence-shell atomic orbitals (NAOs),

$$h_A = \sum_k \quad a_k \, \theta_k^{(A)} \qquad (17)$$

Two valence shell NBOs will result due to the two valence hybrids h_A and h_B ; an in-phase "Lewis-type" NBO (16), and a corresponding out-of-phase "non-Lewis" NBO Ω_{AB}^* .

$$\Omega_{AB}^* = c_B h_A - c_A h_B \qquad (18)$$

The bonding NBOs are of the "Lewis orbital-type", and antibonding NBOs are of the "non-Lewis type". Full Lewis orbitals (2 electrons) are complemented by empty non-Lewis orbitals, in an idealized Lewis structure.

Usually, a one-centre core (CR) and a valence lone pair (LP), and two-centre bond (BD) orbitals are included in a set of Lewis type NBOs whereas, unoccupied valence non-bonding (LP*), and extra-valence-shell Rydberg (RY*) orbitals as well as the valence antibonds (BD*) are included in a non-Lewis set.

NBO analysis is very useful in studying molecular systems. It can be used to investigate the conjugative interactions in molecular systems, to obtain information about the stabilizing interactions between

filled and unoccupied orbitals and destabilizing interactions between filled orbitals etc. The second-order perturbation approach was used to obtain the hypercongugative interaction energy,

$$\Delta E^{(2)}_{i\to j^*} = -n_{\sigma_i} \frac{<\sigma_i|\hat{F}|\sigma_j^*>^2}{\varepsilon_{\sigma_j^*}-\varepsilon_{\sigma_i}} \quad (19)$$

In the above equation, $\hat{F}$ is the Fock operator, $< \sigma_i|\hat{F}|\sigma_j^* >$ is the Fock matrix element between the i^{th} and j^{th} NBO orbitals, $\varepsilon_{\sigma_i} =< \sigma_i|\hat{F}|\sigma_i >$ and $\varepsilon_{\sigma^*} =< \sigma_j^*|\hat{F}|\sigma_j^* >$ are the respective orbital energies of donor and acceptor NBOs and n_σ is the population of the donor σ orbital. As the value increases, the interaction between electron donors and acceptors become more intensive, that is, the extend of conjugation of the system increases [13,14,15,16,17].

2.4 HOMO-LUMO ANALYSIS

The very important and popular quantum mechanical descriptors- HOMO (highest occupied molecular orbital) and LUMO (lowest unoccupied molecular orbital) energies – play a major role in governing many chemical reactions and determining electronic band gaps in solids, and are also responsible for the formation of many charge-transfer complexes. By the frontier molecular orbital theory, the interaction between the frontier orbitals (HOMO and LUMO) of reacting species leads to the formation of a transition state.

The orbitals most likely to be involved in chemical reactions such as the redistribution of electrons (bond creation and destruction, oxidation, and reduction). Since the highest energy orbital HOMO is fully occupied, the removal of electrons from this orbital is the energetically easiest one. This may be simply donating electron density to result in a bond (act as a Lewis base) or may be an oxidation. In contrast, the energetically easiest method to add more electrons is to the low-lying orbital that is empty, LUMO.

HOMO can be seen as the outer orbital containing electrons, and it tend to give these electrons as an electron donor. Hence the ionization potential and the energy of HOMO is directly related. LUMO on the other hand, can accept electrons and hence the LUMO energy directly relates to the electron affinity. This implies that the HOMO-LUMO gap explains the reactivity of the molecule. That is, a molecule with least HOMO-LUMO gap is more reactive while that with a large HOMO-LUMO gap will have high stability (or lower reactivity) [21,22].

HOMO -LUMO analysis and their properties like energy are of much use for material studies, and are very important parameters of quantum chemistry also. It can explain many types of reactions in conjugated systems and are also used in frontier electron density for predicting the most reactive position in π- electron systems.

2.5 UV-VISIBLE SPECTROSCOPY

There are different electronic states (which contains vibrational states, and with which the rotational states exist) associated with a molecule, corresponding to different electronic arrangement and each having different energies. On absorbing or emitting radiations, there can be transitions among these electronic states, for relatively large energy changes which correspond to visible or UV radiations. Alternatively, it can be said as the electronic spectra of a molecule arise from transitions between electronic states of different quantum numbers induced by electromagnetic radiation with UV or visible (UV/vis) light-hence electronic spectra is also called as UV-visible spectra. The electronic excitation can also lead to a change in the shape of the molecule.

In the electronic spectra of molecules in liquid or solid state, the rotational and sometimes vibrational fine structure do not appear. However, the molecular group involved has a characteristic position and intensity of the rather broad absorption due to an electronic transition. The electronic spectrum is divided into three regions for practical reasons as: (1) the visible region between 400 and 750 nm, (2) the near-ultra-violet region, between 200 and 400nm, and (3) the far (or vacuum) ultra-violet, below 200 nm.

The *intensity* of an electronic absorption is given by the Lambert–Beer law:

$$\varepsilon = \frac{1}{cl}\log_{10}\frac{I_0}{I} \qquad (20)$$

where c and l are the concentration and path length of the sample (in $mol\,L^{-1}$ and in cm, respectively), I_0 is the intensity of light of wavelength λ_{max}, falling on the sample, and I is the intensity transmitted by the sample. ε is the molar absorption coefficient and ranges from some 5×10^5 for the strongest bands to 1 or less for very weak absorptions.

The molecular electronic energy levels are shown in figure 2.5.1 below:

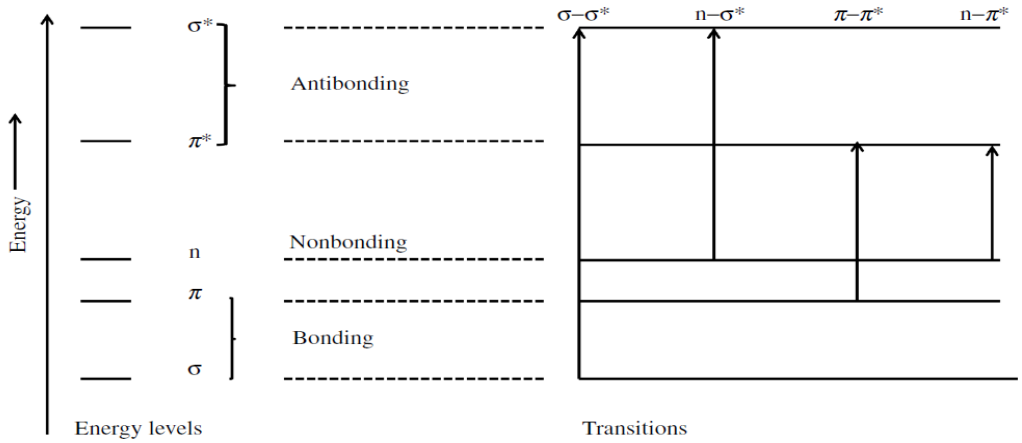

Figure 2.5.1 : Molecular electronic energy levels

Electrons in a vast majority of molecules fall into any one of the three classes: σ electrons,π electrons, and non-bonding electrons (called n electrons). In the bonding of atoms into molecules, the third class do not have any role. In chemical terms, in the atomic single bonds such as $C-C, C-H, O-H$, etc., only σ electrons are involved, where in a multiple bond like $C=C, C\equiv C, C=N$, etc., π electrons are involved in addition, while atoms to the right of C in the periodic table , precisely nitrogen, oxygen, and the halogens, possess n electrons. Generally, σ electrons are most firmly bound to the nuclei and hence they require a great amount of energy to undergo transitions.

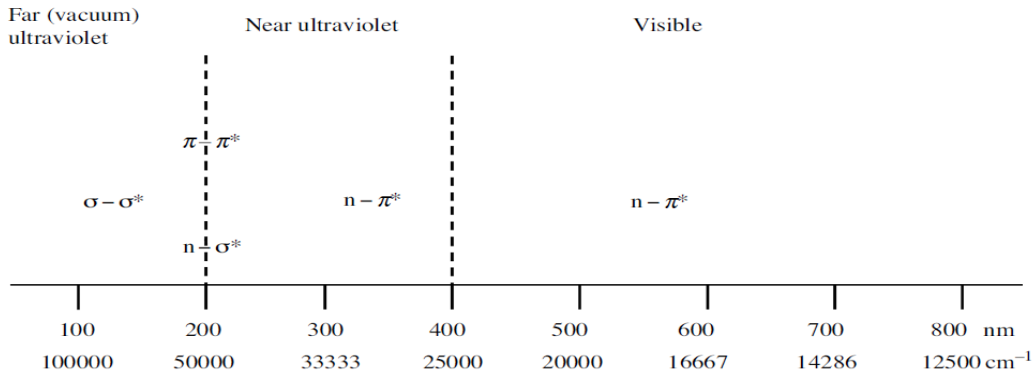

Figure 2.5.2: Regions of the electronic spectrum and the electronic transitions observed

Then the π electron transition energy comes and the least energy is meant for the n electron transitions. Thus, $\sigma \rightarrow \sigma^*$ transitions fall into the vacuum ultra-violet, $\pi \rightarrow \pi^*$ and $n \rightarrow \sigma^*$ appear near the borderline of the near- and far ultra-violet, and $n \rightarrow \pi^*$ come well into the near ultra-violet and visible regions. These are indicated schematically in figure 2.5.2.

The intensities of electronic transitions can be represented by a dimensionless quantity, the oscillator strength (f), which is the ratio of the observed integrated absorption coefficient of a transition to the theoretical value for a fully allowed transition:

$$f = \frac{\underline{A}_{obs}}{\underline{A}_{theor}} \tag{21}$$

Electronic absorption bands with f values near unity indicates that the transitions are fully allowed. Some observed electronic bands have very much smaller values of f, and these are called "forbidden bands" [18,19].

The figure 2.5.3 shows a sample UV spectrum:

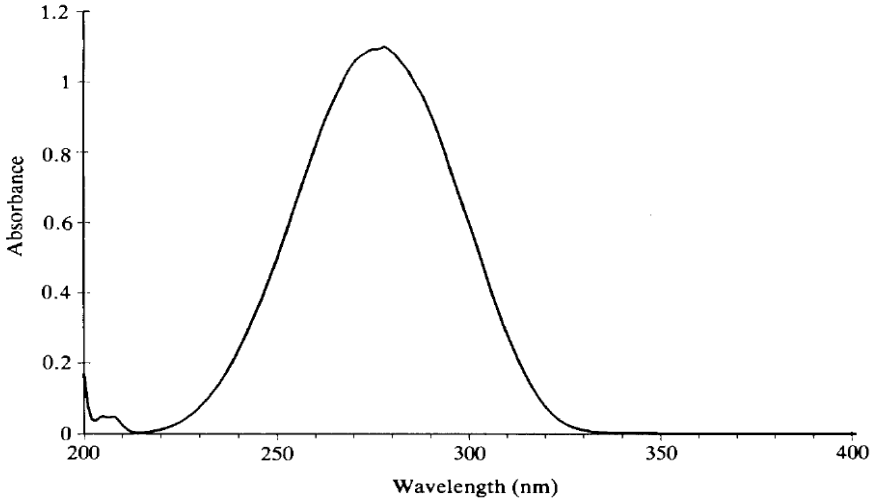

Figure 2.5.3: The ultra-violet spectrum of propanone

Instrumentation

The analysis of various compounds through the use of radiant energy in the UV to visible regions of the electromagnetic spectrum can be done by using a Beckman Model DK-A spectrophotometer (UV-VIS-NIR spectrophotometer) as shown in figure 2.5.4. The analytical information can be obtained in terms of absorbance, reflectance or transmittance of energy in the 200nm-3000nm wavelength range.

In this device, a single beam of energy is chopped into alternative reference and sample beams to provide a double beam system with the sample compartment. Both sample and reference beam have common detection and amplification components. The accessory "Integrating Sphere" with a Lambda-19 spectrometer can be used to analyse samples in reflectance mode, and this helps to analyse samples like cloth, lather, dye-products, films etc. The instrument can also be used to study the kinetic behaviour of chemical reaction with respect to time.

UV-VIS-NIR spectrophotometer uses thin flakes of the grown crystals to obtain the absorption spectra of the single crystal specimens. These flakes are pasted on a thick black paper with a cut exposing the crystal flake to the incident light. A replica of the black paper having a cut at exactly the same position as the crystal flake or a blank glass slide is used as the reference. For reflectance measurement standard aluminium coated mirror can be used in the same place. Since the crystal size is smaller than the sample compartment, this arrangement is necessary. For replica, blank glass slides can also be used.

Figure 2.5.4 UV-VIS-NIR Spectrophotometer (Source-Internet)

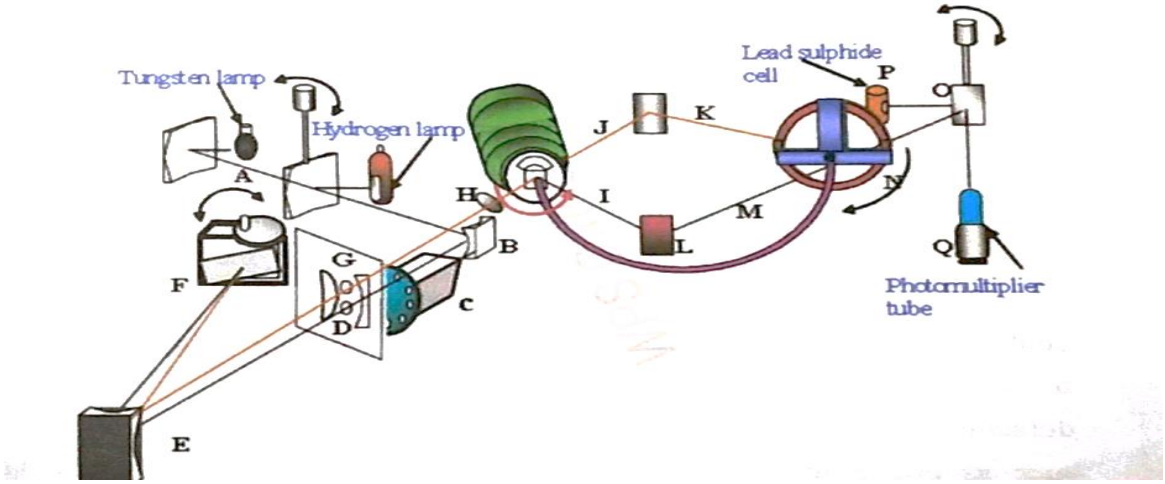

Figure 2.5.5 Optical diagram of spectrophotometer (Source-Internet)

The figure 2.5.5 shows the path followed by a single ray within the radiation beam. From the condensing mirror(A) , the beam is reflected to the slit entrance mirror (B), which directs the beam to the chopper (C). Then, the chopped beam passes through the adjustable entrance slit (D) and into the monochromator. The beam is reflected from the collimating mirror (E) in parallel rays through a reflecting quartz prism (F), which disperses the beam into its spectrum of successive wavelengths. The back surface of the prism is aluminized so that the beam is reflected back through the prism and as it emerges of incidence, it is further dispersed, and enables selection of a particular group of wavelengths that comprise a spectral band. This radiation band is directed back to the collimating mirror, which focusses the entrance slit image on the exit slit (G). The radiant energy, from the monochromator, is directed by lens (H) into the double beam optical system in the sample compartment .The Perkin Elmer, Model: Lambda-19 instrument is double beam ratio recording spectrophotometer i.e., radiant energies transmitted by the reference and sample beam (J and M) are compared, and the ratio of the sample energy of the reference beam is recorded as percentage transmission. The double beam optical system consists of two synchronized semi-circular rotating mirrors (I and N), and two stationary mirrors (L and K) in the sample compartment. The rotating mirrors consequently deflect and pass the radiant energy so that it is directed alternatively into the sample and reference cells 15 (or 12.5) times per second. The energy transmitted by the sample and reference cells are focussed by the detector selector mirror (O) onto the detector [23].

2.6 Z-SCAN TECHNIQUE

The investigations on materials having large yet fast nonlinearities are still accelerating process. This is because the search for materials for all-optical switching and sensor applications, concerns both nonlinear absorption (NLA) and nonlinear refraction (NLR). The Z-scan technique (**Fig.2.6.1**)is a method which can rapidly measure both NLA and NLR in solids, liquids and liquid solutions. The technique as well as its interpretation is simple. The index changes Δn, and absorption change, $\Delta\alpha$ can be determined directly from the data, in most experiments. However, this method is sensitive to all nonlinear optical mechanisms that give rise to a change of the refractive index and/or absorption coefficient, so that the underlying physical processes present from a Z-scan is not possible to determine generally. To unambiguously determine the relevant mechanisms, a series of Z-scans at different pulse widths, frequencies, focal geometries etc. are along with a variety of other experiments are needed [20].

The Z-scan technique are mainly of two types: “closed” and “open” methods (Fig.2.6.2). The open method is typically used in conjunction with the closed method to correct the calculated value, as

nonlinear absorption can affect the measurement of the non-linear index. The Z-scan technique is used in its closed-aperture and open aperture form for measuring the real part and the imaginary part of the nonlinear refractive index respectively. In its closed aperture form, the nonlinear material reacts like a weak z-dependent lens, and the far-field aperture makes it possible to detect the small beam distortions in the original beam. The focussing power of this weak nonlinear lens depends on the nonlinear refractive index and hence, by analysing the z-dependent data acquired by the detector and by cautiously interpreting them using a suitable theory, it is possible to obtain its value. In open-aperture measurements, the far-field aperture is removed and the signal as a whole is measured by the detector. Here, the small beam distortions become insignificant and the z-dependent signal variation is only due to the nonlinear absorption.

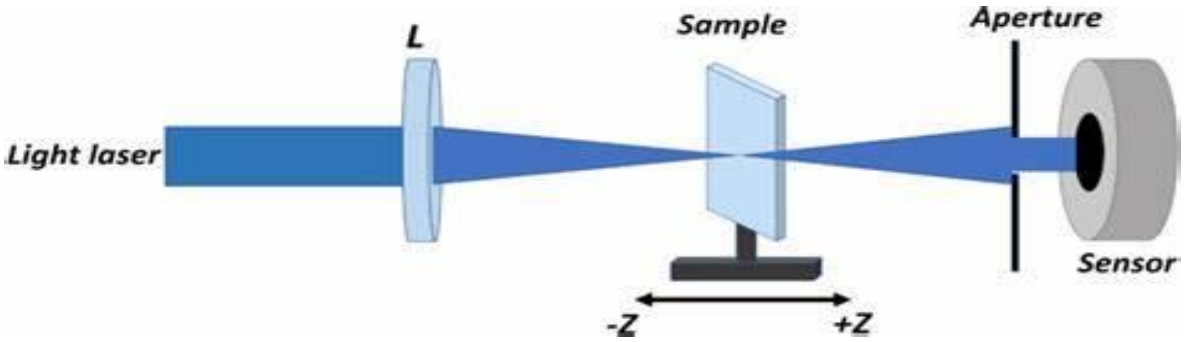

Figure 2.6.1. Schematic diagram of Z-Scan technique (Source-Internet)

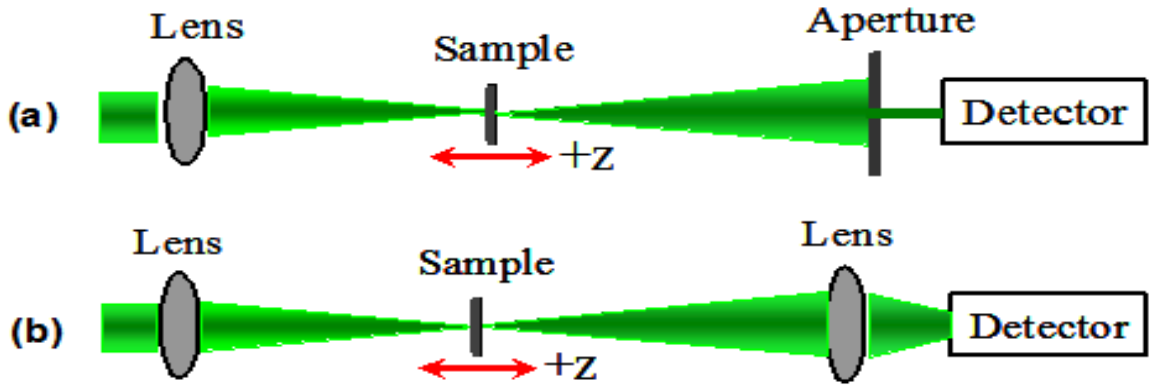

Figure 2.6.2. Schematic diagram of (a) closed aperture and (b)open aperture z-scan techniques (Source-Internet)

2.7 X-RAY DIFFRACTION

X-ray diffraction analysis (XRD) is a technique used in material science for the crystallographic structure determination of a material. In this, the material is irradiated with incident X-rays and then the intensities and scattering angles of the X-rays that leave the material are measured. Information on structures, phases, preferred crystal orientations(texture), and other structural parameters such as average grain size, crystallinity, strain and crystal defects can be obtained from its data. X-ray diffraction peaks are produced by constructive interference of a monochromatic beam of X-rays scattered at specific angles from each set of lattice planes in a sample. The distribution of atoms within the lattice contribute to the peak intensities. Hence, the X-ray diffraction pattern is the fingerprint of periodic atomic arrangements in each material.

The X-rays generated by a cathode ray tube is filtered, collimated, and directed toward the sample. The incident rays on interaction with the sample produces constructive interference obeying the Bragg's Law($n\lambda = 2d\sin\theta$), which relates the wavelength of electromagnetic radiation to the diffraction angle and the lattice spacing in a crystalline sample. These X-rays are the detected, processed and counted. All possible diffraction directions of the lattice can be obtained by changing the geometry of the incident rays, the orientation of the centered crystal and the detector. The angle between the incident and the diffracted rays is the key component of all diffraction even if the instrumentation of Powder and Single-crystal diffraction vary beyond this. By scanning the sample through a range of 2θ angles, all possible diffraction directions of the lattice is obtained due to the random orientation of the powdered material. The diffraction peaks are converted into d-spacings, which allow the identification of the compound because each compound has a unique d-spacings, which are taken as standard values for comparison. The figure 2.7.1 shows the image of a single crystal XRD diffractometer (a) and the schematic diagram of the XRD diffraction(b).

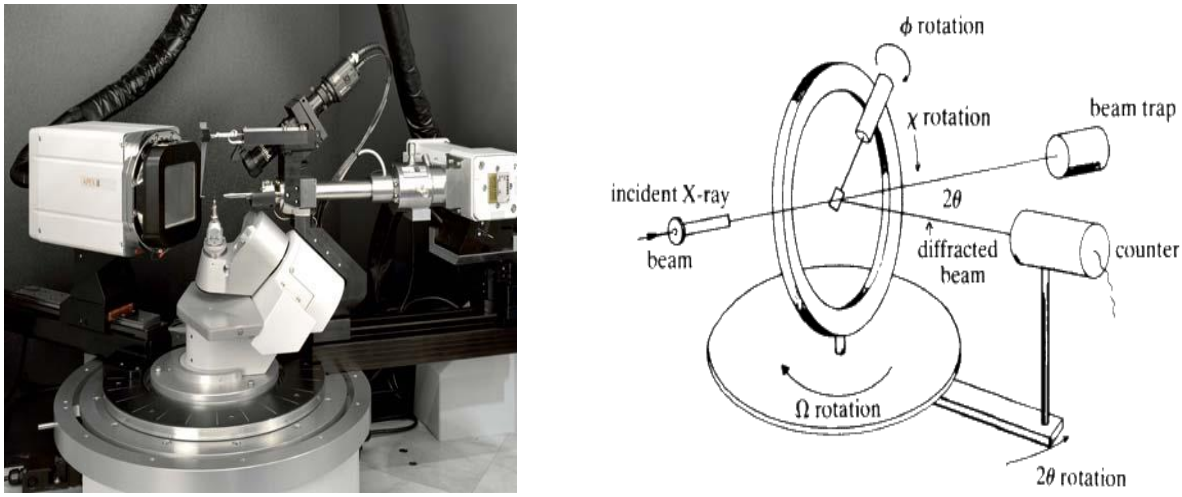

Figure 2.7.1.(a) Single crystal XRD diffractometer- image (b)Schematic diagram of single crystal XRD diffraction(Source-Internet)

The X-ray diffractometers consists of three basic elements: X-ray tube, a sample holder, and an X-ray detector. The X-ray spectra containing several components, mostly K_α, K_β is produced from a cathode tube. K_α in turn consists of $K_{\alpha1}$ and $K_{\alpha2}$, and the specific wavelengths are the characteric of the target material. To produce monochromatic X-rays for diffraction, filtering by foils or crystal monochromators are required, after which they are collimated and directed onto the sample. As the sample and the detector are rotated, the intensity of the X-rays is recorded. When the incident X-ray geometry satisfies the Bragg's law, constructive interference occurs and a peak in intensity appears. A detector records and processes this X-ray signal and converts the signal back to a count rate, which is then output to a device such as a printer or computer monitor [24].

CHAPTER 3

LITERATURE REVIEW

Lynnette Joseph et al. synthesized a new chalcone derivative, 1-(4-aminophenyl)-prop-2-en-1-one (DMAC), and single crystals were grown by slow evaporation technique. FT-IR & Raman spectra, thermogravimetric and UV-Vis studies were carried out. The FT-Raman and FT-IR spectra were interpreted by using normal coordinate analysis following structure optimizations and force field calculations based on density functional theory (DFT) at B3LYP/6-311+G(d,p) level of theory. Typical facilitate calculations were performed utilizing the DFT drive field, rectified by a suggested set of scaling components, yielding reasonably great agreement between the observed and the calculated wave numbers. The thermal stability of DMAC is upto 220°C and in the visible region, it is optically transparent. By mapping electron density isosurface with electrostatic potential surfaces (ESP), information about the size, shape charge density distribution and site of chemical reactivity of the molecule was obtained. This paper reports the SHG effect from a centrosymmetric crystal and the SHG efficiency of the material is found to be 10 times that of standard urea crystal of identical particle size. The crystals grown with good optical properties make DMAC a potential material for photonics device fabrication [25].

M Zarraga et al. reports on their paper the synthesis and the structural analysis of a chalcone derivative of Apocynin,1-(-4-hydroxy-3-methoxyphenyl)-3-(4-nitrophenyl)-2-propenone. The compound was made with a moderately successful outcome (44.6 percentage yield) through Claisen-Schmidt condensation, the main method for the synthesis of chalcones in the presence of an aqueous alkaline base. Single crystal diffraction patterns were recorded with a Bruker SMART AXS CCD diffractometer with graphite-monochromated Mo Ka radiation and semi empirical absorption correction based on symmetry equivalent reflections was applied. PLATON software was used for the structure analysis. The molecular structure is near-planarity, and it allows the molecules to be stacked in columns, at graphite intermolecular distances to each other and connected by a large variety of weak intermolecular interactions. The molecule if found to have structural analogies to related ones with significant pharmacological properties [26].

Vasant S. Naik et al. grew a new organic nonlinear chalcone derivative -1-(5-bromothiophene-2-yl)-3-(3-methoxyphenyl) prop-2-en-1-one (3MO5B2SC) molecule by slow evaporation method for the theoretical as well as the experimental studies. To study the optimized structure of the molecule and

compare with the reported XRD data theoretically, DFT method was used. The experimental and computed FTIR and H1 NMR spectrum studies confirmed the structure of the molecule. The thermal properties of the molecule like the melting point (117 C) and thermal stability (273 C) were obtained by DSC, TGA, DTA, and DTG.From the optical absorption spectrum, the molecule has lower cut-off wavelength of 410 nm as from UV-Vis-NIR spectrophotometer and 480 nm calculated by DFT. The band gap obtained from the experimental data and the theoretical HOMO-LUMO plots was the same (3.3 eV). The global chemical reactivity descriptor (GCRD) was calculated. Using a diode-pumped continuous wave Nd-YAG laser at 532 nm wavelength the non-linear parameters like nonlinear absorption coefficient, nonlinear refraction index, and third order nonlinear susceptibilities and hyper polarizability were measured. The experimental and theoretical nonlinear parameters are found as many times higher than that of urea molecule. The nonlinearity displayed by the molecule exploited for studying its optical constraining factor. The results regarding its structure and the properties show that the material of interest is a good choice for NLO device applications [27].

Vasant S. Naik *et al* performed both theoretical and experimental studies on the crystal structure and NLO properties of three thiophenyl chalcones-, B5B2SC, 3C5B2SC. and 2M5B2SC. The single-crystal XRD method was used to determine the crystal structures and confirmation of the structures were made by using experimental and theoretical FTIR and ^{1}H NMR spectra. High thermal stability, wide transparency in the visible region, and small optical band gaps etc. were the key features of these chalcones. Third order NLO parameters such as nonlinear absorption coefficient, nonlinear refractive index, third order NLO susceptibility, molecular hyperpolarizability, ground state absorption cross section and excited state cross sections were determined from the continuous wave (CW) laser Z-scan experimental data analyses. For CW laser at 532 nm wavelengths, the chalcones exhibited optical limiting and optical switching. The electric dipole moment, polarizability, hyperpolarizability, HOMO-LUMO energy gap, global chemical reactivity descriptors (GCRD), molecular electrostatic potentials (MEP) and NBO analysis were computed theoretically using DFT. Geometry optimization was done using B3LYP/6-311+G (d, p) level of the theory. The results showed that these kinetically stable molecules showed large response towards NLO property, and are potential materials for applications as optical devices [28].

Mahesh Pal Singh Yadav *et al* describe the combined theoretical and experimental studies on the molecular structure, vibrational spectra, HOMO-LUMO analysis, and hyperpolarizability of organic nonlinear crystal 3-(3,4-dimethoxyphenyl)-1-(pyridin- 2-yl)prop-2-en-1-one (DPP). DFT using 6-31G(d,p) basis set and Becke's three-parameter hybrid functional (B3LYP) were used to calculate the vibrational wavenumbers with Raman intensities and IR absorption intensities in the ground state.

Intramolecular bonding, bond interactions, and delocalization of unpaired electrons were studied using NBO analysis. Fock matrix, on the second-order perturbation theory analysis revealed the strong intramolecular hyperconjugations of π electrons between π bond orbitals and anti-bonding orbitals. From the calculated HOMO and LUMO energies, global reactivity descriptors such as energy band gap, chemical potential, etc. were calculated. Optical and nonlinear properties were studied by using UV spectra and first hyperpolarizability calculations. The results showed that DPP is suitable NLO applicant [29].

S. Sebastian and Gowtha N. Sundaraganesan reported a combined experimental and theoretical study on the molecular structure, vibrational spectra, NBO and UV analysis of 4-Hydroxypiperidine (4-HP). The DFT methods (BLYP, B3LYP) with 6-311G (d, p) basis set were used to study the molecular geometry, harmonic vibrational frequencies and bonding features. The normal coordinate analysis (NCA), followed by the Scaled Quantum Mechanical Force Field (SQMFF), assigned the vibrational spectra. NBO analysis has been done to study the stability of the molecule arising from hyperconjugative interactions and charge delocalization. Charge transfer occurring within the molecule was revealed by the calculated HOMO and LUMO energies. The observed spectra and the simulated IR and Raman spectra of the compound with its calculation results were in good agreement [30].

P. V Sreelaja et al. theoretically studied the optimized geometry, vibrational spectra, frontier molecular orbitals of the compound-2- amino-3-nitopyridinium 4-hydroxybenzenesulfonate. It was a DFT study using Gaussian ’09 program. NBO theory was used to investigate on the second order interactions of Lewis and non- Lewis orbitals which quantifies the charge transfer interaction, and the stability of the molecule. FTIR and FT-Raman studies were carried out and then by using potential energy distribution, the vibrational contribution to each normal mode was determined. By utilizing Natural atomic charges, MEP mapping and frontier molecular orbital analysis, the electronic properties and chemical activity were studied. The active frontier molecular orbitals responsible for the electronic transitions were identified. Evaluation of the dipole moment and second order polarizability was also done. All these results confirmed the existence of nonlinear properties of the molecule [31].

Amit Kumar et al. on their paper reports the combined experimental and theoretical studies on FT-IR, FT-Raman, NMR, UV–vis spectra of a chalcone derivative (2E)-3- [4(methylsulfa- nyl) phenyl]-1-(4-nitrophenyl) prop-2-en-1-one (4N4MSP). The structural optimizations and normal coordinate force field calculations were done based on the DFT theory with B3LYP functional and 6-311++G(d,p) basis set combination, and the molecular structure, fundamental vibrational frequencies and intensity of the bands were explained. The fundamental modes were analysed using potential energy

distribution(PED). For predicting sites and relative reactivities towards electrophilic and nucleophilic attack, MEP surface was plotted over the geometry and by NBO analysis, the delocalization of electron densities of various constituents of the molecule. Using the time-dependent DFT(TD-DFT), the electronic properties- excitation energies, oscillator strength, wavelengths, HOMO-LUMO energies were determined and the results were found contrary to the experimental values. The NLO parameters like dipole moment, mean polarizability, anisotropy of polarizability, and first order hyperpolarizability etc. of the molecule were calculated based on the finite-field approach. A good NLO behaviour of the molecule is highlighted by the predicted first order hyperpolarizability values [32].

Tongpeng Zhao et al. synthesized a new promising NLO material 1-(-4-methoxyphenyl)-3-(4-N, N dimethyl aminophenyl)-2-propen-1-one(DAMO). Its high-quality crystal was grown by slow evaporation technique. The single crystal XRD revealed the structure of the crystal and the FTIR and ^{1}H NMR spectroscopy confirmed all the functional groups of the crystal. The experimental data on the thermal, optical and dielectric properties of the crystal were analysed systematically. The SEM and AFM images were used to study the surface morphology. The HOMO-LUMO energy gap value was theoretically found out by using Gaussian 09 package. The SHG efficiency of DAMO was obtained as 42.71 times that of KDP crystal, and was confirmed by the Kurtz-Perry powder technique [33].

Kai Xu et al. in their work, designed two novel chalcone derivative crystals with non-centrosymmetric structures, 6MN3MPP($C_{21}H_{18}O_3PCa_{21}$) and 6MN4MPP($C_{21}H_{18}O_3Pn$), and grew by extending the – conjugation and structure-modifying strategy. The SHG efficiency, thermal stability, transmission spectra, dielectric constant and photoluminescence properties were characterized on this basis and the hyperpolarizability of the crystal was theoretically calculated. The crystals exhibited higher crystal transparency, higher melting point, and lower dielectric constant compared to other chalcone NLO crystals. The SHG intensity of the 6MN3MPP crystal was found to be 4.3 times higher than that of the KDP crystal. All of the outcome showed that the above new compounds are good applicants as NLO crystals [34].

Leonardo R. Almeida et al. reports that they synthesized a new 2-amino-chalcone and by using the single crystal X-ray diffraction technique, the crystal molecular structure was determined. The compound $C_{15}H_{12}BrNO_2$ was found to crystallize in monoclinic centrosymmetric space group C2/c. The Hirshfeld surface analysis showed the presence of hydrogen bonds of types N-H…O and O-H…O that stabilize two independent centrosymmetric dimers, and also that of π-π stacking interactions that stabilize a supramolecular trimeric system. The NLO properties of the 2-amino-chalcone asymmetric unit was studied using the supermolecule approach in combination with an iterative electrostatic

polarization scheme. For dynamic and static cases, the CAM-B3LYP/6-311+G(d) level of theory was used to perform the calculations. In contrast to the crystal form, the 2-amino-chalcone lacks an inversion center when in solution , so that the second order NLO properties do not vanish. Hence, the NLO properties were also computed by the implicit solvation approach IEF-PCM. As the solvent polarity increases, the effect of the solvent on NLO properties was to augment its values. The results showed that the material is interesting substrate for third order NLO applications [35].

In this paper**, *J. Christina Jebapriya et al***. synthezised a novel chalcone derivative (2E)-1-(4-chlorophenyl)-3-(4-diethylaminophenyl)-prop-2-en-1-one (CPDAPP) and it twas crystallized by slow evaporation growth method. The monoclinic system of the compound with P2/c space group was confirmed by the single crystal X-ray diffraction analysis. The FT-IR, FT-Raman, ^{1}H NMR and ^{13}C-NMR studies confirmed the molecular structure. The crystal transparency was studied using UV-Vis spectrum analysis and the value of band gap was obtained as 2.7 eV. Thermal stability, material decomposition and melting point of the grown crystals were investigated by thermos-gravimetric analysis and DSC measurements. The emission peaks, as observed in the photoluminescence spectrum was in the green region. The third order nonlinear optical properties of the crystal was studied in DMF using Z-scan technique with continuous wave (CW) DPSS laser at 532 nm wavelength. Under the CW regime, the compound of interest showed significant two-photon absorption, negative nonlinear refraction and optical limiting threshold. The experimental results were compared with the theoretical results obtained by DFT. The optimized geometry and frontier molecular orbitals were calculated by using B3LYP/6-31++G(d,p) level of theory.. The electronic excitation energies and HOMO-LUMO band gap were also determined by DFT. The experimental and theoretical results were in good agreement, which reveals that the title molecule is a good NLO applicant [36].

V. M. Bhumannavar et al., on their paper confirms the structure of the (E)-1-(4-Chlorophenyl)-3-(4-methylphenyl) prop-2-en-1-one experimentally. The experimentally observed results of FTIR, proton NMR, UV-Visible are compared with theoretically(DFT) obtained results. The decomposition and melting point of the compound is obtained by TGA and DTA. The DFT for the compound was performed using B3LYP/6-311++G(d,p) basis set.TD-DFT was calculated for 3 different methods-B3LYP, Hartree-Fock, and CAMB3LYP also employed for the MLCC at 6-311++G(d,p) basis set. The nonlinear parameters of the molecule were also studied [37].

N. H. Norwawi et al. concentrated on the synthesis of a novel chalcone derivative, (E)-1-(benzo[d][1,3] dioxol-5-yl)-3-(2-chloro-6-fluorophenyl) prop-2-en-1-one (BCFC) , by Claisen-Schmidt condensation method with a mixture of 2-chloro-6-fluorobenzaldehyde and 1-(benzo[d][1,3]dioxol-5-yl)ethenone.

The molecular structure of BCFC, from the single crystal X-ray diffraction analysis, shows s-cis configuration with respect to the enone moity and further stabilized via intramolecular C-H•••F interaction. The BCFC has planar structure which helps to increase its charge transfer within the molecules. There is no significant interaction observed, which is further confirmed by the Hirshfeld fingerprint plot analysis. DFT method with B3LYP /6-311++G(d,p) basis set was used to calculate the optimized molecular structure at the ground state, the molecular electrostatic potential(MEP) and HOMO-LUMO energy band of BCFC was also found. The carbonyl group region at the enone bridge of BCFC shows the electrophilic attack side and acts as a good acceptor part. The BCFC is a good future optoelectronic material with the aid of the small HOMO-LUMO energy gap(2.33 eV) [38].

In the studies of ***Elizabeth Mathew et al***., reports a dual approach on theoretical and experimental studies of nonlinear optical properties of a new chalcone derivative, (2E)-1-(Anthracen-9-yl)-3-(biphenyl-4-yl) prop-2-en-1-one[biphenyl-ANC]. The observations were confirmed by the DFT calculations. The FT-IR, FT-Raman, and UV-visible absorption spectra were recorded and analysed. The B3LYP level of theory with 6-311++G(d,p) basis set was employed for the structural, electronic and charge transfer analyses. The B3LYP and CAM-B3LYP hybrid functional predicted the second-order hyperpolarizability theoretically. By z-scan technique using Q-switched Nd: YAG laser with 5ns pulses at 53 nm , the third-order NLO properties , in addition to the optical limiting studies of the title compound in polar and nonpolar solvents were carried out. The z-scan results establish the compound as a promising candidate for photonic and optoelectronic applications [39].

CHAPTER 4

MATERIALS AND METHODS

A single-crystal or monocrystalline solid is a material in which the crystal lattice of the entire sample is continuous and unbroken to the edges of the sample, with no grain boundaries. The technique of purification which yields a solid phase single compound in a high state of purity by a kinetically controlled process of nucleation in a supersaturated or supercooled solution containing numerous compounds or a melt of several compounds is called crystallization. The process of arranging atoms, ions, molecules or molecular assemblies into regular 3-D periodic arrays is known as the crystal growth. The phase transformation of the solid, liquid or vapour state into the solid state resulted in the growth of single crystals. One of the major criteria for the success of crystallization is the solubility of the chemical compound that involved in the process. The solubility of a chemical compound is the maximum amount / concentration of that compound that can dissolve in a specific solvent system. When the solute concentration in the solvent is a maximum at the solubility limit at which there is no further dissolution, and concentration change occur in the solution, the solution is said to be saturated. The solution becomes supersaturated when the solute concentration exceeds its solubility limit, at the equilibrium condition at a given temperature.

In crystal growth , first-order phase transitions in which there is a coexistence of two distinct uniform phases that are stable at the equilibrium point and separated by an interface phase boundary are involved. The phases can exist near the equilibrium point, one as thermodynamically stable phase and the other as the thermodynamically metastable phase. The metastable phase is supersaturated(supercooled) with respect to the stable(equilibrium)phase, and as a result a thermodynamic driving force of crystallization will appear leading at a critical value of supersaturation to spontaneous nucleation of the crystalline phase within the metastable fluid phase. By providing a seed crystal or a substrate in contact with the fluid phase, a controlled propagation of the solid/fluid phase boundary occurs.

When two phases are in equilibrium, the Gibb's potential of the phases, G1 and G2 are equal so that the potential difference between the phases is zero. For a single component system at uniform temperature and pressure,

$$G_1=U_1+PV_1-TS_1$$

$$G_2=U_2+PV_2-TS_2$$

$$G_1-G_2=\Delta G=\Delta U+P\Delta V-T\Delta S$$

Where $\Delta U=\Delta H-P\Delta V$, is the change in internal energy.

Relatively small volume change is involved in a melt-solid phase transition.i.e., $\Delta V\approx 0$.Then at phase equilibrium, the Helmholtz free energy F:

$$\Delta F=\Delta G_{V,P=constant}=\Delta H-T_e\,\Delta S=0$$

Where ΔH=enthalpy released by crystallization(latent heat of fusion), ΔS=the transition (melting) entropy,& T_e = the equilibrium temperature(melting point).

The essential requirement for crystallization of a stable solid phase within a metastable fluid phase is the deviation from the thermodynamic equilibrium (crossing of coexisting conditions between the phases). The variation of chemical potential near two-phase equilibrium is shown in Fig.4.1.

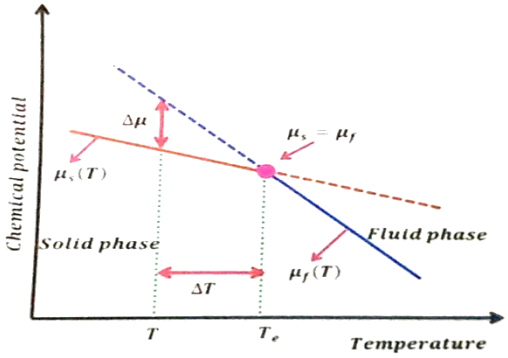

Figure 4.1. Variation of chemical potential near two-phase equilibrium

Crystal growth is a diffusion and integration process in which the solute molecules or ions enter the growing faces of a crystal by diffusion, convection, or a combination of both mechanisms through the liquid phase. At the surface these solute molecules or ions are organized into the crystal lattice through an adsorbed layer by surface integration. The formation of a crystal from the initially disordered phase involves three basic features: supersaturation, supercooling and nucleation.

The essential driving force for crystallization and for higher-quality crystals of that compound is the supersaturation or supercooling of liquid or gas phase with respect to the chemical compound required for growth. The supersaturated solution is thermodynamically unstable. The supersaturation required for crystallization can be achieved by slow evaporation, slow cooling and by adding any external impurity. Among these, slow cooling is the best method to grow bulk size crystals by solution technique, where the crystallization takes place by lowering the temperature of the solution under a controlled cooling rate. For materials having very small temperature coefficient of solubility, the method of slow evaporation of the solvent can be used. The addition of some impurities also leads to supersaturation. The growth proceeds by the reduction of solubility of the solute due to the impurity presence. The shape of the solubility curve determines the suitable growth method.

The process of formation of centres of crystallization such as the minute solid bodies, embryos, nuclei or seeds in the supersaturated solution for the overall crystallization process is called nucleation. When a few atoms or molecules join together in a supersaturated/supercooled system, a change in free energy takes place in the cluster formation in new phase known as embryo. The cluster consisting of such atoms or molecules is called a nucleus. There is a greater probability for the nucleus to grow if it grows to a particular size known as 'critical size'(critical nucleus).The four stages of the formation of a stable nucleus are:

i. The development of saturated stage, which may be due to a chemical reaction, a change in pressure, temperature or any other chemical or physical condition.
ii. The generation of nucleus
iii. The growth of nucleus from the unstable state to stable state or to the critical size.
iv. The relaxation process where the texture of the new phase changes

Nucleation may occur spontaneously or it may be induced artificially. Also, it can be homogeneous, in the absence of foreign particles or crystals in the solution, or heterogeneous, in the presence of foreign particles in the solution. Both types are collectively known as primary nucleation. The secondary nucleation is referred to the formation of nuclei in the vicinity of crystals of the solute in the supersaturated solution, the presence of the solute crystals nucleates the supersaturated solution at a lower supersaturation.

Organic NLO molecules are crystallized based on solution growth, melt growth or vapour growth, depending upon the production of either 3-D bulk, 2-D platelet, and 1-D fiber-like crystals. The low-temperature solution growth close to the thermodynamic equilibrium is the most common way to obtain high optical quality organic crystals. The driving force for crystallization in all the crystal growth

methods is the difference in chemical potential ($\Delta\mu$) of the material in the liquid or vapour phase and that in the solid. ($\Delta\mu = \mu_f - \mu_s$).

By solvent evaporation, supersaturation at a constant temperature can be continuously maintained for the growth of crystals. As it requires only a low temperature gradient, this method is mostly used for aqueous and organic solutions.

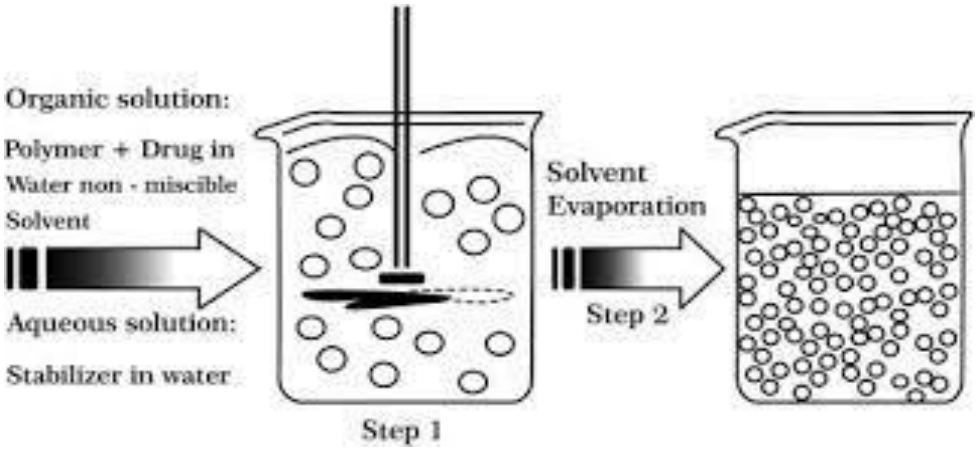

Figure 4.2. Solvent evaporation technique (Source-Internet)

The merits of the flux evaporation method are:

- Homogeneous concentration of dopants and impurities.
- Homogeneous density of equilibrium defects
- No variation in the composition in the case of solid solution
- Possibility of growing materials having a specified valence state.

Controlling the evaporation rate which depends on the temperature, and removing the solvent vapours are some of its major disadvantages.

CHAPTER 5

RESULT AND DISCUSSION

5.1 SYNTHESIS

The (2E)-2-(3,4-Dimethoxybenzylidene)-3,4-dihydronaphthalen-1(2H)-one was synthesized using equimolar quantities of 3,4- dimethoxy benzaldehyde (0.015 mol) and α-tetralone (0.015 mol) were dissolved in ethanol in a 250 ml conical flask and stirred for 15 min. The solution mixture was again stirred for 1 hour after adding freshly prepared 10 % NaOH and the mixture was kept at room temperature for 24 h and then poured into ice-cold water. A yellow precipitate was obtained and washed several times with distilled water to remove any vestige of NaOH. The filtered, dried crude product was recrystallized from acetone solution. After four days, yellow block crystals were obtained.

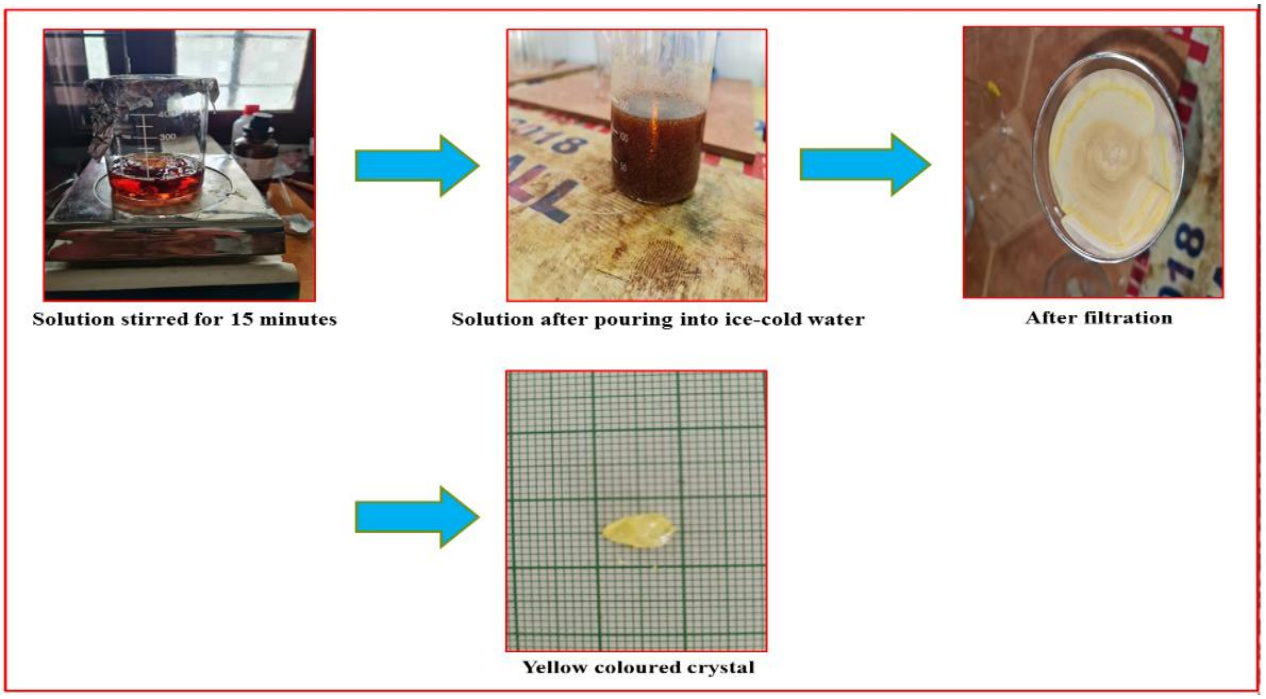

Figure 5.1 synthesis of (2E)-2-(3,4-Dimethoxybenzylidene)-3,4-dihydronaphthalen-1(2H)-one

5.2 CRYSTAL STRUCTURE AND OPTIMIZED GEOMETRY

The single crystal X ray diffraction analysis has been set out to investigate the interactions which are described in **Table 5.2**.1 It has been confirmed that (2E)-2-(3,4-Dimethoxybenzylidene)-3,4-

dihydronaphthalen-1(2H)-one belongs to the Orthorhombic crystal system in the $P2_12_12_1$ space group with cell parameters a=7.8906(7) Å, b=9.4104(8) Å and c=20.7764(19) Å,α=90°, β=90° and γ=90° in tune with its reported structure [40].The structure was solved by direct method procedures as implemented in SHELXS2008 program.

Table5.2.1. Crystallographic data and structure refinement for (2E)-2-(3,4-Dimethoxybenzylidene)-3,4-dihydronaphthalen-1(2H)-one)

Empirical Formula	$C_{19}H_{18}O_3$
Formula Weight	294.33
Temperature	296(2) K
Wavelength	0.71073 Å
Crystal System	Orthorhombic
Space Group	$P2_12_12_1$
Unit Cell Dimensions	a = 7.8906(7) Å α = 90° b = 9.4104(8) Å β = 90° c = 20.7764(19) Å γ = 90°
Z	4
Volume	1542.7(2) $Å^3$
Density	1.267 g/cm^3
Absorption coefficient	0.085 mm^{-1}
F (000)	624
Crystal Size	0.350 x 0.400 x 0.450 mm
Theta range for data collection	2.92 to 28.46°
Index ranges	-10<=h<=10, -11<=k<=11, -27<=l<=27
Reflections collected	17019
Independent reflections	3824 [R(int) = 0.0503]
Refinement method	Full-matrix least-squares on F^2
Data/Restraints/Parameters	3824 / 0 / 202
Goodness-of-fit on F^2	1.037
Final R indices [I > 2sigma(I)]	R1 = 0.0413
	wR2 = 0.0956
R indices (all data)	R1 = 0.0531
	wR2 = 0.1029
Largest diff. peak and hole	0.168 and -0.164 $eÅ^{-3}$

Table 5.2.2. Optimized geometric parameters of (2E)-2-(3,4-Dimethoxybenzylidene)-3,4-dihydronaphthalen-1(2H)-one

Bond Lengths (Å)	CCPVTZ	X-ray	Bond Angles (°)	CCPVTZ	X-ray	Dihedral Angles (°)	CCPVTZ	X-ray
O_1-C_6	1.3586	1.35708	C_6-O_1-C_{33}	118.4867	118.26	C_{33}-O_1-C_6-C_4	-0.2847	1.2978
O_1-C_{33}	1.4167	1.41045	C_9-O_2-C_{37}	118.4498	117.48	C_{33}-O_1-C_6-C_9	179.2502	-178.41
O_2-C_9	1.3540	1.36193	H_5-C_4-C_6	119.0061	119.48	C_6-O_1-C_{33}-H_{34}	179.7851	177.85
O_2-C_{37}	1.4185	1.40923	H_5-C_4-C_{14}	119.4442	119.53	C_6-O_1-C_{33}-H_{35}	-61.4535	-62.18
O_3-C_{18}	1.2224	1.21897	C_6-C_4-C_{14}	121.4915	120.97	C_6-O_1-C_{33}-H_{36}	61.0421	57.82
C_4-H_5	1.0763	0.93019	O_1-C_6-C_4	124.8709	125.12	C_{37}-O_2-C_9-C_6	-179.2104	173.55
C_4-C_6	1.3835	1.37582	O_1-C_6-C_9	115.3369	115.21	C_{37}-O_2-C_9-C_7	-0.1075	-6.19
C_4-C_{14}	1.4107	1.39672	C_4-C_6-C_9	119.7906	119.64	C_9-O_2-C_{37}-H_{38}	179.9821	-177.22
C_6-C_9	1.4159	1.39949	H_8-C_7-C_9	120.1227	120.01	C_9-O_2-C_{37}-H_{39}	-61.2361	-57.192
C_7-H_8	1.0792	0.93016	H_8-C_7-C_{11}	119.3073	120.21	C_9-O_2-C_{37}-H_{40}	61.2058	62.83
C_7-C_9	1.3884	1.36995	C_9-C_7-C_{11}	120.5669	119.77	H_5-C_4-C_6-O_1	1.8252	0.9017
C_7-C_{11}	1.3903	1.38162	O_2-C_9-C_6	115.8378	115.58	H_5-C_4-C_6-C_9	-177.6905	-179.39
C_{10}-C_{16}	1.3492	1.33387	O_2-C_9-C_7	125.1519	124.42	C_{14}-C_4-C_6-O_1	179.0336	-179.07
C_{10}-C_{18}	1.4957	1.48785	C_6-C_9-C_7	119.0044	119.99	C_{14}-C_4-C_6-C_9	-0.482	0.6291
C_{10}-C_{22}	1.5083	1.50105	C_{16}-C_{10}-C_{18}	116.2371	116.81	H_5-C_4-C_{14}-C_{11}	175.8756	178.99
C_{11}-H_{21}	1.0816	0.93019	C_{16}-C_{10}-C_{22}	126.237	126.41	H_5-C_4-C_{14}-C_{16}	-1.8926	1.907
C_{11}-C_{14}	1.3953	1.38473	C_{18}-C_{10}-C_{22}	117.5216	116.73	C_6-C_4-C_{14}-C_{11}	-1.3209	-1.027
C_{13}-C_{15}	1.4014	1.39151	C_7-C_{11}-H_{12}	119.2566	119.2	C_6-C_4-C_{14}-C_{16}	-179.0891	-178.11
C_{13}-C_{18}	1.4934	1.47741	C_7-C_{11}-C_{14}	121.4233	121.56	O_1-C_6-C_9-O_2	0.9363	-0.605
C_{13}-C_{25}	1.3976	1.39648	H_{12}-C_{11}-C_{14}	119.3166	119.23	O_1-C_6-C_9-C_7	-178.225	179.151
C_{14}-C_{16}	1.4566	1.45608	C_{15}-C_{13}-C_{18}	121.1335	121.18	C_4-C_6-C_9-O_2	-179.5033	179.66
C_{15}-C_{19}	1.504	1.49738	C_{15}-C_{13}-C_{25}	120.0022	119.41	C_4-C_6-C_9-C_7	1.3354	-0.58
C_{15}-C_{27}	1.3936	1.38667	C_{18}-C_{13}-C_{25}	118.8584	119.39	H_8-C_7-C_9-O_2	-0.0871	0.626
C_{16}-H_{17}	1.085	0.9296	C_4-C_{14}-C_{11}	117.6812	118.02	H_8-C_7-C_9-C_6	178.9897	-179.1
C_{19}-H_{20}	1.0953	0.97045	C_4-C_{14}-C_{16}	124.3514	123.84	C_{11}-C_7-C_9-O_2	-179.4384	-179.31
C_{19}-H_{21}	1.0911	0.97068	C_{11}-C_{14}-C_{16}	117.9314	118.06	C_{11}-C_7-C_9-C_6	-0.3616	0.9484
C_{19}-C_{22}	1.5323	1.51548	C_{13}-C_{15}-C_{19}	119.3652	119.29	H_8-C_7-C_{11}-H_{12}	-0.174	-1.287
C_{22}-H_{23}	1.0966	0.96939	C_{13}-C_{15}-C_{27}	118.9344	119.29	H_8-C_7-C_{11}-C_{14}	179.1339	178.66
C_{22}-H_{24}	1.0885	0.96953	C_{19}-C_{15}-C_{27}	121.6824	121.68	C_9-C_7-C_{11}-H_{12}	179.1826	178.65
C_{25}-H_{26}	1.0808	0.92972	C_{10}-C_{16}-C_{14}	131.59	130.81	C_9-C_7-C_{11}-C_{14}	-1.5095	-1.392
C_{25}-C_{29}	1.3842	1.36805	C_{10}-C_{16}-H_{17}	114.0668	114.57	C_{18}-C_{10}-C_{16}-C_{14}	176.9503	179.08
C_{27}-H_{28}	1.0831	0.93034	C_{14}-C_{16}-H_{17}	114.3348	114.6	C_{18}-C_{10}-C_{16}-H_{17}	-4.1808	-0.954
C_{27}-C_{31}	1.3882	1.37707	O_3-C_{18}-C_{10}	122.328	121.44	C_{22}-C_{10}-C_{16}-C_{14}	-3.8326	-3.05
C_{29}-H_{30}	1.0817	0.93087	O_3-C_{18}-C_{13}	120.1951	120.35	C_{22}-C_{10}-C_{16}-H_{17}	175.0363	176.9
C_{29}-C_{31}	1.3931	1.37226	C_{10}-C_{18}-C_{13}	117.4663	118.16	C_{16}-C_{10}-C_{18}-O_3	-6.1127	-11.8
C_{31}-H_{32}	1.0822	0.93039	C_{15}-C_{19}-H_{20}	109.1994	109.11	C_{16}-C_{10}-C_{18}-C_{13}	175.0726	170.43
C_{33}-H_{34}	1.0866	0.96046	C_{15}-C_{19}-H_{21}	110.0941	109.2	C_{22}-C_{10}-C_{18}-O_3	174.5993	170.12
C_{33}-H_{35}	1.0934	0.95931	C_{15}-C_{19}-C_{22}	111.9318	112.21	C_{22}-C_{10}-C_{18}-C_{13}	-4.2153	-7.6414
C_{33}-H_{36}	1.0935	0.95961	H_{20}-C_{19}-H_{21}	106.452	107.87	C_{16}-C_{10}-C_{22}-C_{19}	-141.6309	-138.39
C_{37}-H_{38}	1.0864	0.96029	H_{20}-C_{19}-C_{22}	108.8753	109.16	C_{16}-C_{10}-C_{22}-H_{23}	97.6826	100.49
C_{37}-H_{39}	1.0931	0.95966	H_{21}-C_{19}-C_{22}	110.1241	109.15	C_{16}-C_{10}-C_{22}-H_{24}	-19.9309	-17.31
C_{37}-H_{40}	1.0930	0.95986	C_{10}-C_{22}-C_{19}	111.9463	111.97	C_{18}-C_{10}-C_{22}-C_{19}	37.5773	39.46
			C_{10}-C_{22}-H_{23}	110.0463	109.17	C_{18}-C_{10}-C_{22}-H_{23}	-83.1093	-81.64
			C_{10}-C_{22}-H_{24}	110.2047	109.19	C_{18}-C_{10}-C_{22}-H_{24}	159.2773	160.55
			C_{19}-C_{22}-H_{23}	108.4557	109.24	C_7-C_{11}-C_{14}-C_4	2.3196	1.40982
			C_{19}-C_{22}-H_{24}	109.1669	109.21	C_7-C_{11}-C_{14}-C_{16}	-179.7658	178.66

			H_{23}-C_{22}-H_{24}	106.8725	107.94	H_{12}-C_{11}-C_{14}-C_4	-178.3729	-178.63
			C_{13}-C_{25}-H_{26}	118.1136	119.55	H_{12}-C_{11}-C_{14}-C_{16}	-0.4583	-1.378
			C_{13}-C_{25}-C_{29}	120.5206	120.85	C_{18}-C_{13}-C_{15}-C_{19}	-1.0418	-2.2575
			H_{26}-C_{25}-C_{29}	121.3659	119.58	C_{18}-C_{13}-C_{15}-C_{27}	-179.525	179.22
			C_{15}-C_{27}-H_{28}	119.4135	119.68	C_{25}-C_{13}-C_{15}-C_{19}	178.0633	177.21
			C_{15}-C_{27}-C_{31}	120.7683	120.46	C_{25}-C_{13}-C_{15}-C_{27}	-0.4199	-1.295
			H_{28}-C_{27}-C_{31}	119.8182	119.85	C_{15}-C_{13}-C_{18}-O_3	165.726	170.06
			C_{25}-C_{29}-H_{30}	120.2312	120.24	C_{15}-C_{13}-C_{18}-C_{10}	-15.4328	-12.146
			C_{25}-C_{29}-C_{31}	119.5952	119.49	C_{25}-C_{13}-C_{18}-O_3	-13.3891	-9.41
			H_{30}-C_{29}-C_{31}	120.1736	120.26	C_{25}-C_{13}-C_{18}-C_{10}	165.452	168.37
			C_{27}-C_{31}-C_{29}	120.1767	120.75	C_{15}-C_{13}-C_{25}-H_{26}	-179.3603	-179.21
			C_{27}-C_{31}-H_{32}	119.779	119.6	C_{15}-C_{13}-C_{25}-C_{29}	0.604	0.83
			C_{29}-C_{31}-H_{32}	120.0441	119.63	C_{18}-C_{13}-C_{25}-H_{26}	-0.235	0.2725
			O_1-C_{33}-H_{34}	105.8881	109.42	C_{18}-C_{13}-C_{25}-C_{29}	179.7294	-179.68
			O_1-C_{33}-H_{35}	111.5918	109.46	C_4-C_{14}-C_{16}-C_{10}	-26.1037	-35.42
			O_1-C_{33}-H_{36}	111.5715	109.49	C_4-C_{14}-C_{16}-H_{17}	155.0298	144.61
			H_{34}-C_{33}-H_{35}	109.2425	109.5	C_{11}-C_{14}-C_{16}-C_{10}	156.1333	147.48
			H_{34}-C_{33}-H_{36}	109.2363	109.46	C_{11}-C_{14}-C_{16}-H_{17}	-22.7332	-32.47
			H_{35}-C_{33}-H_{36}	109.2234	109.46	C_{13}-C_{15}-C_{19}-H_{20}	-85.4181	-86.29
			O_2-C_{37}-H_{38}	105.8628	109.45	C_{13}-C_{15}-C_{19}-H_{21}	158.0484	156
			O_2-C_{37}-H_{39}	111.4813	109.44	C_{13}-C_{15}-C_{19}-C_{22}	35.2123	34.83
			O_2-C_{37}-H_{40}	111.4677	109.52	C_{27}-C_{15}-C_{19}-H_{20}	93.022	92.170
			H_{38}-C_{37}-H_{39}	109.3218	109.48	C_{27}-C_{15}-C_{19}-H_{21}	-23.5115	-25.51
			H_{38}-C_{37}-H_{40}	109.3234	109.44	C_{27}-C_{15}-C_{19}-C_{22}	-146.3476	-146.69
			H_{39}-C_{37}-H_{40}	109.301	109.47	C_{13}-C_{15}-C_{27}-H_{28}	-179.9493	-178.75
						C_{13}-C_{15}-C_{27}-C_{31}	-0.0259	1.1940
						C_{19}-C_{15}-C_{27}-H_{28}	1.6041	2.7640
						C_{19}-C_{15}-C_{27}-C_{31}	-178.4726	-177.18
						C_{15}-C_{19}-C_{22}-C_{10}	-52.4163	-52.47
						C_{15}-C_{19}-C_{22}-H_{23}	69.1895	68.558
						C_{15}-C_{19}-C_{22}-H_{24}	-174.7105	-173.54
						H_{20}-C_{19}-C_{22}-C_{10}	68.4023	68.620
						H_{20}-C_{19}-C_{22}-H_{23}	-169.9919	-170.31
						H_{20}-C_{19}-C_{22}-H_{24}	-53.892	-52.440
						H_{21}-C_{19}-C_{22}-C_{10}	-175.2353	-173.68
						H_{21}-C_{19}-C_{22}-H_{23}	-53.6296	-52.61
						H_{21}-C_{19}-C_{22}-H_{24}	62.4704	65.24
						C_{13}-C_{25}-C_{29}-H_{30}	179.558	179.78
						C_{13}-C_{25}-C_{29}-C_{31}	-0.3331	-0.229
						H_{26}-C_{25}-C_{29}-H_{30}	-0.4788	-0.177
						H_{26}-C_{25}-C_{29}-C_{31}	179.6301	179.81
						C_{15}-C_{27}-C_{31}-C_{29}	0.296	-0.605
						C_{15}-C_{27}-C_{31}-H_{32}	-179.5898	179.38
						H_{28}-C_{27}-C_{31}-C_{29}	-179.781	179.34
						H_{28}-C_{27}-C_{31}-H_{32}	0.3333	-0.6600
						C_{25}-C_{29}-C_{31}-C_{27}	-0.1158	0.1130
						C_{25}-C_{29}-C_{31}-H_{32}	179.7696	-179.87
						H_{30}-C_{29}-C_{31}-C_{27}	179.993	-179.89
						H_{30}-C_{29}-C_{31}-H_{32}	-0.1215	0.112

The optimized structural parameters of (2E)-2-(3,4-Dimethoxybenzylidene)-3,4-dihydronaphthalen-1(2H)-one calculated using the B3LYP/cc-PVTZ basis set are listed in Table 5.2.1 along with the experimental data, correspondingly with the atom numbering scheme in Fig. 5.2.2. The title compound is composed of three fragments: Dimethoxy phenyl ring, Cyclohexane ring and phenyl ring. This is due to the repulsion between the carbon atom in the ring and the electron cloud of hydrogen atoms of the CH_3 substituent. The angle C_7-C_9-O_2 is increased by 5.0^0 resulting from the repulsion between the lone pairs of O_2 and O_1. The parameters obtained from the computation are found to be comparable with the XRD data as understood from the linear regression analysis shown in **Fig.5.2.1**, with R2 values of 0.9923, 0.9712 and 0.9925 for the fit of bond lengths, bond angles and dihedral angles respectively and the optimized structure is shown in **Fig.5.2.2**.

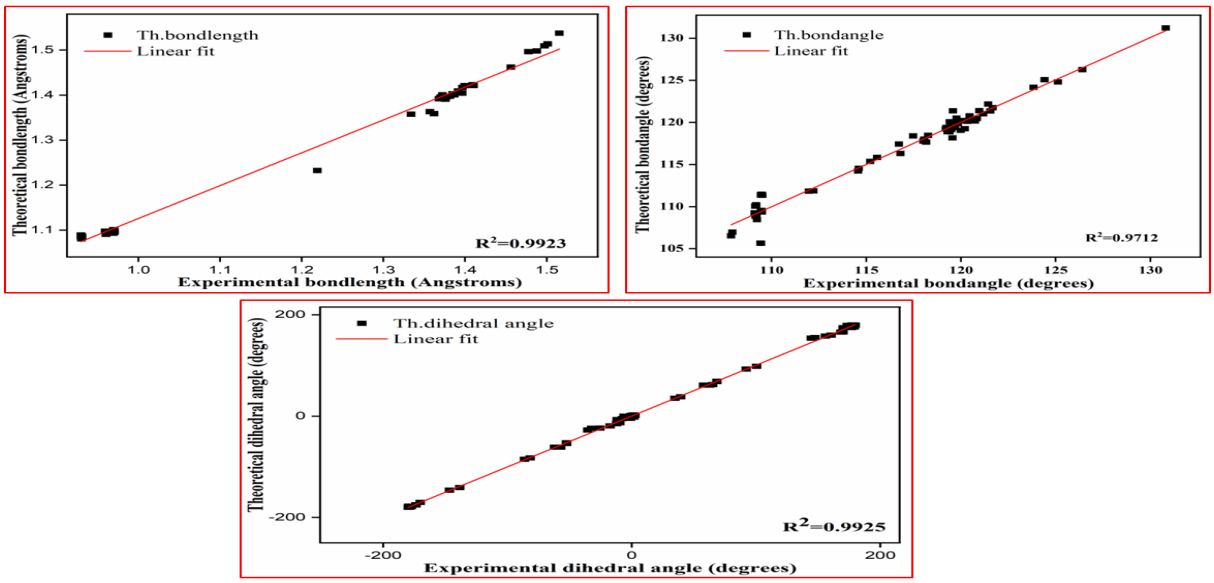

Figure 5.2.1 Linear Regression for bond parameters of (2E)-2-(3,4-Dimethoxybenzylidene)-3,4-dihydronaphthalen-1(2H)-one

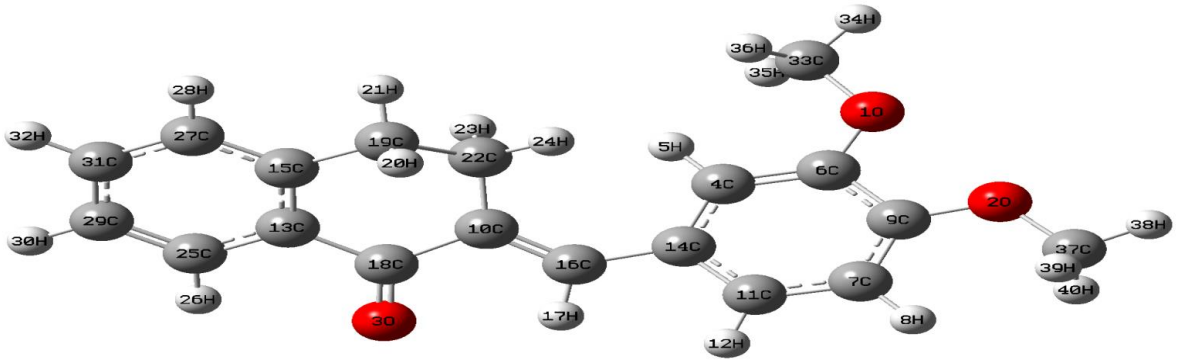

Figure 5.2.2 Optimized Geometry of (2E)-2-(3,4-Dimethoxybenzylidene)-3,4-dihydronaphthalen-1(2H)-one at the B3LYP/cc-PVTZ level.

5.3 NATURAL BOND ORBITAL ANALYSIS

Natural bond orbital (NBO) consider the electronic wave work by implies a set of Lewis and non-Lewis localized orbitals. Concise account of the NBO sections utilized and their geometrical importance has been analysed with the NBO 3.1 program (Glendening et al., University of Wisconsin, Madison, WI, USA). The NBO analysis permits the energy calculation without electron delocalization but with the same identical geometry. The increased stabilization energy associated with delocalization $E^{(2)}$ shows an intensive interaction between electron donors and electron acceptors. The upgrade of $E^{(2)}$ also predicts a more prominent degree of conjugation effect in the entire system [41].

Table 5.3.1. Second-order perturbation theory analysis of Fock matrix in natural bond orbital basis

Donor (i)	ED (i) [e]	Acceptor (j)	ED (j) [e]	E(2)[a] [Kj/mol^{-1}]	E(j)-E(i)[b] [a.u]	F(i, j)[c] [a.u]
		π*(C7-C9)	0.38351	72.55056	0.29	0.064
π(C_4-C_6)	1.71583	π*(C11-C14)	0.38099	75.22832	0.3	0.067
		π*(C4-C6)	0.36025	72.29952	0.29	0.064
π(C_7-C_9)	1.68261	π*(C11-C14)	0.38099	83.72184	0.3	0.07
π(C_{10}-C_{16})	1.82675	π*(O3-C18)	0.209	88.82632	0.29	0.07
		π*(C4-C6)	0.36025	78.49184	0.27	0.064
		π*(C7-C9)	0.38351	80.66752	0.27	0.065
π(C_{11}-C_{14})	1.65513	π*(C10-C16)	0.13665	64.09888	0.3	0.064
		π*(O_3-C_{18})	0.209	80.3328	0.27	0.067
		π*(C_{25}-C_{29})	0.28951	86.31592	0.28	0.07
π(C_{13}-C_{15})	1.62125	π*(C_{27}-C_{31})	0.3225	76.39984	0.28	0.064
		π*(C_{13}-C_{15})	0.37506	76.48352	0.29	0.065
π(C_{25}-C_{29})	1.65758	π*(C_{27}-C_{31})	0.3225	93.63792	0.28	0.071
		π*(C_{13}-C_{15})	0.37506	93.7216	0.29	0.073
π(C_{27}-C_{31})	1.66271	π*(C_{25}-C_{29})	0.28951	72.34136	0.29	0.064
LP(2)(O_1)	1.83845	π*(C_4 - C_6)	0.36025	130.1642	0.34	0.097
LP(2)(O_2)	1.82827	π*(C_7-C_9)	0.38351	134.139	0.34	0.098
		σ*(C_{10}-C_{18})	0.07253	84.64232	0.67	0.105
LP(2)(O_3)	1.88255	σ*(C_{13}-C_{18})	0.06916	84.39128	0.67	0.105
		π*(C_{10}-C_{16})	0.13665	145.645	0.03	0.071
π*(O_3-C_{18})	0.209	π*(C_{13}-C_{15})	0.37506	526.7656	0.01	0.07
π*(C_4-C_6)	0.36025	π*(C_{11}-C_{14})	0.38099	1017.884	0.01	0.077
π*(C_7-C_9)	0.38351	π*(C_{11}-C_{14})	0.38099	829.4362	0.02	0.079
π*(C_{11}-C_{14})	0.38099	π*(C_{10}-C_{16})	0.13665	244.764	0.02	0.064
π*(C_{27}-C_{31})	0.3225	π*(C_{13}-C_{15})	0.37506	1136.625	0.01	0.083

ED: electron density; i: donor orbital; j: acceptor orbital; e: occupancy; a. u: arbitrary unit

[a]Energy of hyperconjugative interactions

[b]Energy difference between donor and acceptor i and j natural bond orbitals

[c]Fock matrix element between i and j natural bond orbitals

In the Phenyl ring, π (C_{27}-C_{31}) bond conjugates with, π*(C_{25}-C_{29}) and π*(C_{15}-C_{13}) leading to a stabilization energy of 72.34 and 93.72 kj/mol^{-1} respectively. The π (C_{25}-C_{29}) bond which further conjugates with π*(C_{27}-C_{31}) and π*(C_{15}-C_{13}) contributes an additional energy of 93.63 and 76.48 kj/mol^{-1}. Significant amount of hyper conjugative interactions between π (C_4-C_6) and π*(C_{11}-C_{14}) leads to a stabilization energy of 75.22 kj/mol^{-1}. This enhanced π*(C_4-C_6) NBO further conjugates with π*(C_{11}-C_{14}) resulting in an enormous $E^{(2)}$ energy of 1017.88 kj/mol^{-1}.similarly, π(C_{27}-C_{31}) conjugate with π*(C_{15}-C_{13}) and π*(C_{27}-C_{31}) conjugate with π*(C_{15}-C_{13}) leading to a stabilization of 93.72 and 1136.62 kj/mol^{-1}. The intramolecular hyperconjugative interactions due to orbital overlap between LP (O) and π*(C-C) bond orbitals which results in ICT causing stabilization of the system. The lone pair interaction energy for LP (O_1) → π*(C_4-C_6) and LP (O_2) → π*(C_9-C_7) are 130.16 and 134.03 kj/mol^{-1} respectively. So there is an increase in energy and shortening of corresponding C-O bonds give clear idea about resonance of the asymmetric tri-substituted phenyl ring (Ph2) is increased by the electron donating oxygen atoms.

5.4 ULTRAVIOLET–VISIBLE SPECTROSCOPY

The solvent effect of (2E)-2-(3,4-Dimethoxybenzylidene)-3,4-dihydronaphthalen-1(2H)-one was calculated using PCM–TD-DFT method by employing the B3LYP/cc-pVTZ functional. The observed and simulated UV–vis spectra in acetone are shown in Figure 5.4. The results are given in **Table 5.4**. The experimental absorption spectrum in acetone gives a strong transition at 349 nm which is due to the n→π* transition and a high transmittance percentage in the entire visible region (380–800 nm) makes (2E)-2-(3,4-Dimethoxybenzylidene)-3,4-dihydronaphthalen-1(2H)-one a good candidate for NLO applications. The computed spectrum taken in acetone medium provides a strong transition at 395.91 nm with strong oscillator strength 0.5550. The computed spectrum gives transitions at 395.91,361.24, 319.54 nm with energy 302.15, 331.14, 374.37 kJ/mol-1 respectively. This shows the presence of bathochromic shift. This says that shift of a substance to lower energy state with a longer wavelength. The computed transition energy is shifted because of the charge transfer interaction.

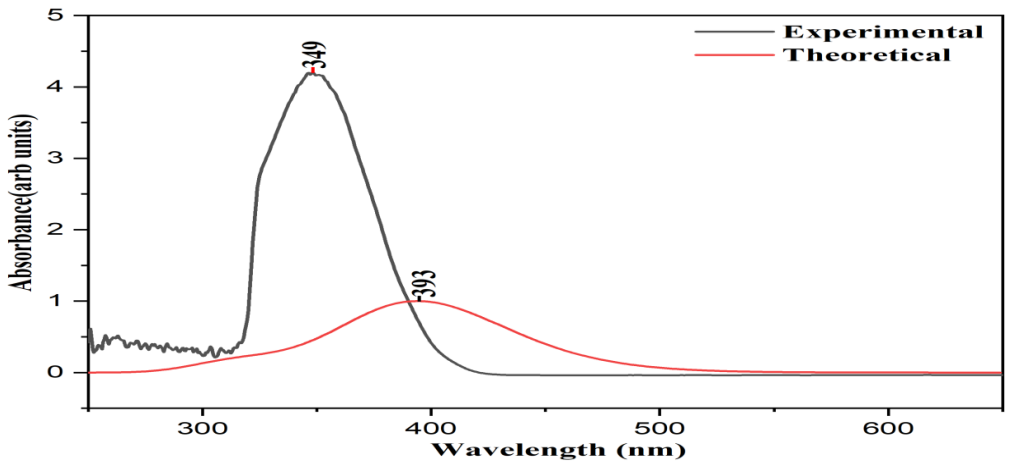

Fig 5.4 UV-Vis spectrum of (2E)-2-(3,4-Dimethoxybenzylidene)-3,4-dihydronaphthalen-1(2H)-one

Table 5.4 Experimental and calculated absorption wavelengths, energies and oscillator strengths of(2E)-2-(3,4-Dimethoxybenzylidene)-3,4-dihydronaphthalen-1(2H)-one using the TD-DFT method at the B3LYP/cc-pVTZ

Excitation	CI expansion coefficient	Wavelength (nm)		Wavelength (eV)	Oscillator strength (f)
		Cal.	Exp.		
Excited State 1 78 -> 79	Singlet-A 0.69628	395.91	-	3.1316	0.5550
Excited State 2 74 -> 79 75 -> 79 76 -> 79	Singlet-A 0.18455 0.30693 0.58596	361.24	349	3.4321	0.0305
Excited State 3 77 -> 79	Singlet-A 0.68933	319.54	-	3.8801	0.1083

5.5 FRONTIER MOLECULAR ORBITAL ANALYSIS

Frontier molecular orbitals are inevitable parameters in quantum chemistry because they alter the way the molecule interacts with other species [42]. The HOMO energy, LUMO energy and HOMO-LUMO gap in (2E)-2-(3,4-Dimethoxybenzylidene)-3,4-dihydronaphthalen-1(2H)-one are calculated to be -8.033 eV, -5.9184 eV and 2.1146 eV respectively. The illustrated representation of HOMO calculated

using B3LYP/cc-PVTZ functional suggests that the charge density is localized predominantly over the dimethoxy phenyl ring and in LUMO the charge concentrates over the cyclohexane ring, which indicate the charge transfer interaction [43,44] leading to nonlinear optical properties in (2E)-2-(3,4-Dimethoxybenzylidene)-3,4-dihydronaphthalen-1(2H)-one.

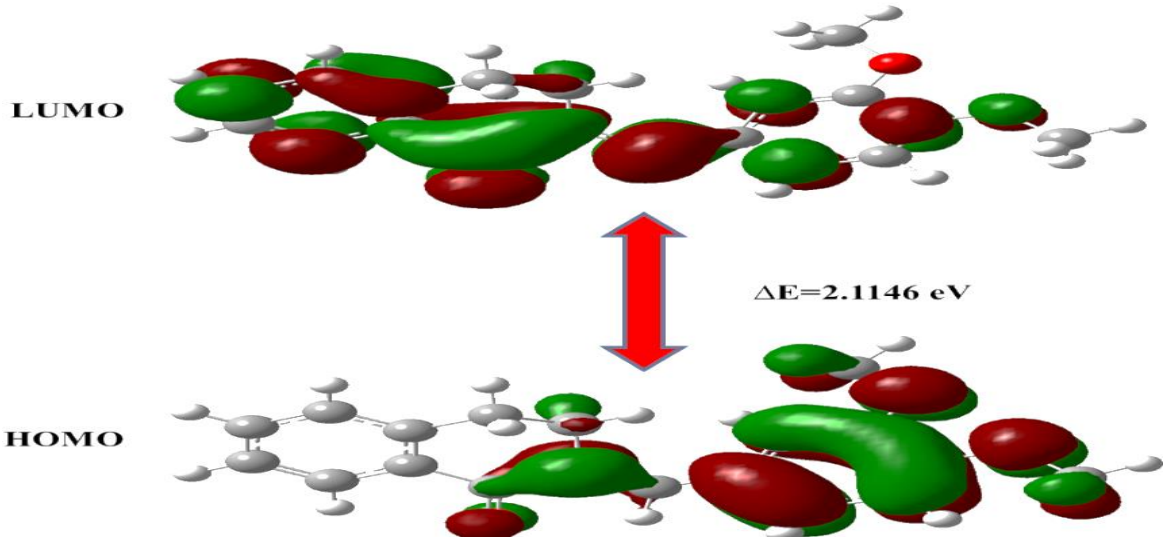

Figure 5.5.1 HOMO-LUMO plot of (2E)-2-(3,4-Dimethoxybenzylidene)-3,4-dihydronaphthalen-1(2H)-one

The energy difference has much importance in electro-optic properties and stability of the compound. A system having Lower energy gap labelled is more reactive or less stable and Higher values point out more hardness or less softness of a compound [45].

5.6 VIBRATIONAL SPECTRAL ANALYSIS

A visual comparison of the simulated IR and experimental IR spectra are dissipated in Figure 5.6.1. Vibrational assignments were performed at B3LYP/cc-PVTZ level of theory. The title compound is composed of three fragments: Dimethoxy Phenyl ring, Cyclohexane ring and one phenyl ring. The compound consists of Phenyl ring vibrations, Carbonyl group vibrations, Methoxy group vibrations and Methyl group vibrations. Vibrational assignments are given in **Table 5.6.1**

5.6.1. Carbonyl group vibrations

One of the most extensively studied bands is provided by the carbonyl group vibrations though it provides characteristic band in the whole spectrum [46]. Carbonyl stretching vibrations of saturated esters is expected to be in the range 1750-1735 cm^{-1}. The calculated wavenumber of 1664 cm^{-1} as a

medium intensity peak and the strong intensity peak in IR spectrum at 1666 cm^{-1} are assigned to the C=O stretching mode. This downgrade of carbonyl stretching wavenumbers is due to the conjugation of C=O bond with the aromatic ring [47].

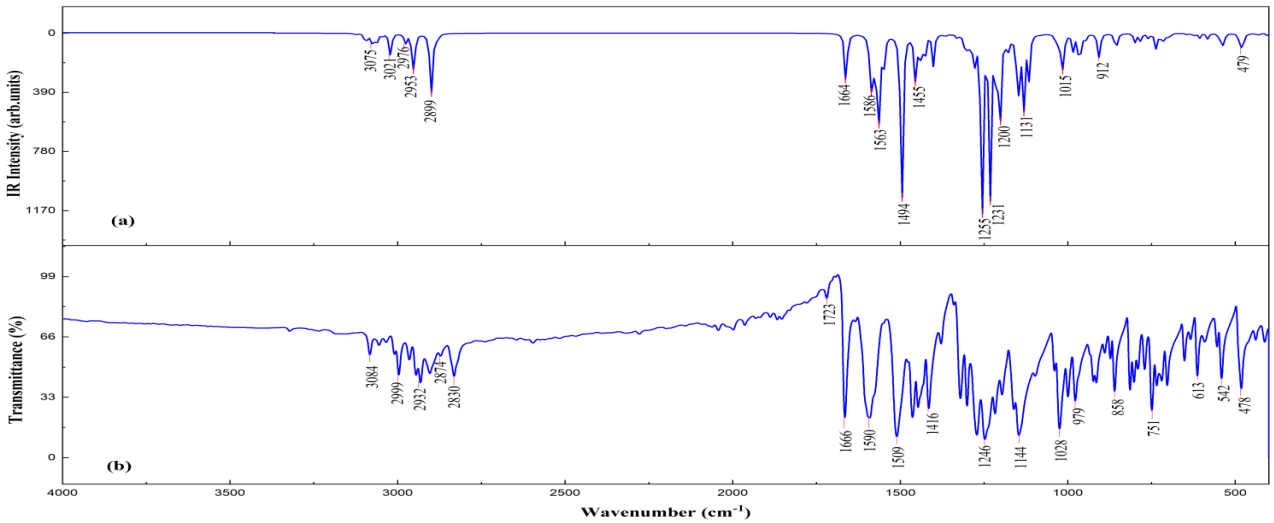

Figure 5.6.1 (a) Experimental FT-IR spectra in the range 4000-400 cm^{-1} and (b) Simulated IR spectra of (2E)-2-(3,4-Dimethoxybenzylidene)-3,4-dihydronaphthalen-1(2H)-one by B3LYP/cc-PVTZ level of theory.

5.6.2. Vibrations of Phenyl ring

For all the aromatic compounds the carbon-hydrogen stretching vibrations are expected to be in the range 3100-3000 cm^{-1}. The (2E)-2-(3,4-Dimethoxybenzylidene)-3,4-dihydronaphthalen-1(2H)-one is composed by one phenyl ring (Ph1) associated to cyclohexanone ring and an asymmetric tri-substitution (Ph2). The ring C-H stretching vibrations of Ph1 is observed at 3084 cm^{-1} as a weak peak and computed respectively at 3075, 3021 cm^{-1}. The C-H stretching modes are observed to be weak, owing to the charge transfer from the hydrogen atoms to the carbon atoms. The ring stretching vibrations are observed to be strong: shifting of bands to lower wavenumbers in a response to heavy substituents the number of substituents is on the ring, absorption regions will be broader [48]. DFT computation gives medium peak at 1563 cm^{-1} and strong peak at 1494 cm^{-1} corresponding to ring Ph1 and Ph2. The same is observed as a strong band in IR at 1590 cm^{-1}. Normally, in-plane and out-of-plane C–H bending vibrations are occurring in the region 1300–1000 cm^{-1} and 1000–750 cm^{-1}, respectively. The C-H in-plane bending vibrations observed as a medium peak at 1015 cm^{-1} from computation and strong peak at 1028 cm^{-1} in IR spectrum. The computed out-of-plane C–H bending vibrations are observed at 912 cm^{-1} as a weak band.

5.6.3. Methyl group vibrations

The substituent that commits electron donating especially in the aromatic ring system are Methyl group. The asymmetric and symmetric stretching modes of the CH_3 group are expected to occur about 2962 and 2872 cm^{-1} [49]. The methyl symmetric stretching vibration is active in IR as a weak band at 2830 cm^{-1}. The computed result shows a strong peak at 2899 cm^{-1}. The weak band at 2953 cm^{-1} from computed result shows the methyl asymmetric stretching vibrations.

5.6.4. Methoxy group vibrations

The C-H stretching and bending bands are highly influenced when a CH_3 group is directly attached to oxygen atom, results in shifting of position due to electronic effects [50]. The asymmetric bending vibrations of methoxy groups are expected to appear around 1460 cm^{-1} [46]. The medium intensity band at 1464 cm^{-1} in the IR spectrum is assigned to CH_3 asymmetric bending mode. The computed result obtained at 1455 cm^{-1} as a weak band.

5.6.5. Methylene group vibrations

The methylene group asymmetric and symmetric stretching bands expected to be appear at 2926 and 2853 cm^{-1} [49]. The symmetric stretching mode of methylene group of (2E)-2-(3,4-Dimethoxybenzylidene)-3,4-dihydronaphthalen-1(2H)-one is observed as a very weak band in IR at 2874 cm^{-1}. The computed result for asymmetric stretching mode observed at 2976 cm^{-1} as a weak band.

Table 5.6.1 Vibrational assignment of (2E)-2-(3,4-Dimethoxybenzylidene)-3,4-dihydronaphthalen-1(2H)-one

Wavenumbers		Assignments
Experimental IR [cm^{-1}]	Theoretical IR [cm^{-1}]	
3084	3075 3021	Ph1CHss
2830	2899	CH_3ss
-	2953	CH_3 as
2874	-	CH_2 ss
-	2976	CH_2 as
1590	1563 1494	Ph1CC ss Ph2CC ss
1460 1028	1455 1025	CH_3 as CH sb
-	912	CH opb

Stretching; ss: symmetric stretching; as: asymmetric stretching; ips: in plane stretching; ops: out of plane stretching; sb: symmetric bending; b/d: bending; opb: out of plane bending

5.7 NONLINEAR OPTICAL STUDIES

Theoretical investigations have been considered as an impressive tool to match up the crystal properties and structural weirdness. The static and dynamic first and second order hyperpolarizabilities (β and γ) of (2E)-2-(3,4-Dimethoxybenzylidene)-3,4-dihydronaphthalen-1(2H)-one have been calculated using the B3LYP/6-31G basis set in Gaussian 09 program. The dipole moment(μ_{total}), the static (α(0,0)) and frequency dependent (α(-ω,ω)) values of the isotropic (αtotal) and anisotropic (Δα) polarizabilities, static first hyperpolarizability (β(0;0,0)), dynamic first hyperpolarizabilities for electro optic Pockel's effect (β(-ω;ω,0)) and second harmonic generation (β(-2ω;ω,ω)), static second hyperpolarizability (γ(0;0,0)) and dynamic second hyperpolarizabilities for quadratic electro optic Kerr effect (γ(-ω,ω,0,0)) and electric field induced second harmonic generation (γ(-2ω;ω,ω,0)) were computed for the laser wavelength of 532 nm (ħω=0.0857 a.u.) and compared with standard nonlinear crystal urea as given in **Table 5.7.1**.

Table 5.7.1: Standard nonlinear optical parameters of Urea

Nonlinear optical Parameters		Title Compou	Urea
μ_{total} (Debye)		3.208	3.432
α(0,0)x10^{-24} esu	αtotal	34.051	4.942
	Δα	37.247	0.689
α(-ω,ω)x10^{-24} esu	αtotal	40.419	4.995
	Δα	52.929	0.682
β(0; 0,0) x10^{-30} esu		43.151	0.756
β(−ω;ω,0) x10^{-30} esu		161.144	0.922
γ(0; 0,0,0) x10^{-36} esu		98.876	4.023

It is found that static first hyperpolarizability of (2E)-2-(3,4-Dimethoxybenzylidene)-3,4-dihydronaphthalen-1(2H)-one is 57 times that of urea and the dynamic first hyperpolarizabilities for electro optic Pockel's effect are 175 times that of urea. Similarly, static second hyperpolarizability of the title compound is found to be 24.5 times that of urea. The increment of the hyperpolarizability values, which provides an idea about the potential NLO behaviour of (2E)-2-(3,4-Dimethoxybenzylidene)-3,4-dihydronaphthalen-1(2H)-one accredited to electron transfer through its strongly π conjugated system, which is conceivable from NBO analysis.

5.7.1. Z-scan Studies under continuous wave laser excitation

The (2E)-2-(3,4-Dimethoxybenzylidene)-3,4-dihydronaphthalen-1(2H)-one crystal was stick it to z-scan under a continuous laser beam from a semiconductor continuous wave laser of 532 nm wavelength

and 100mW power. The optical path length used was 823 mm with a beam waist radius of 3 mm. The open and closed aperture z-scan curves of (2E)-2-(3,4-Dimethoxybenzylidene)-3,4-dihydronaphthalen-1(2H)-one under continuous wave illumination are shown in **Fig.5.7.1** and **Fig 5.7.2.**

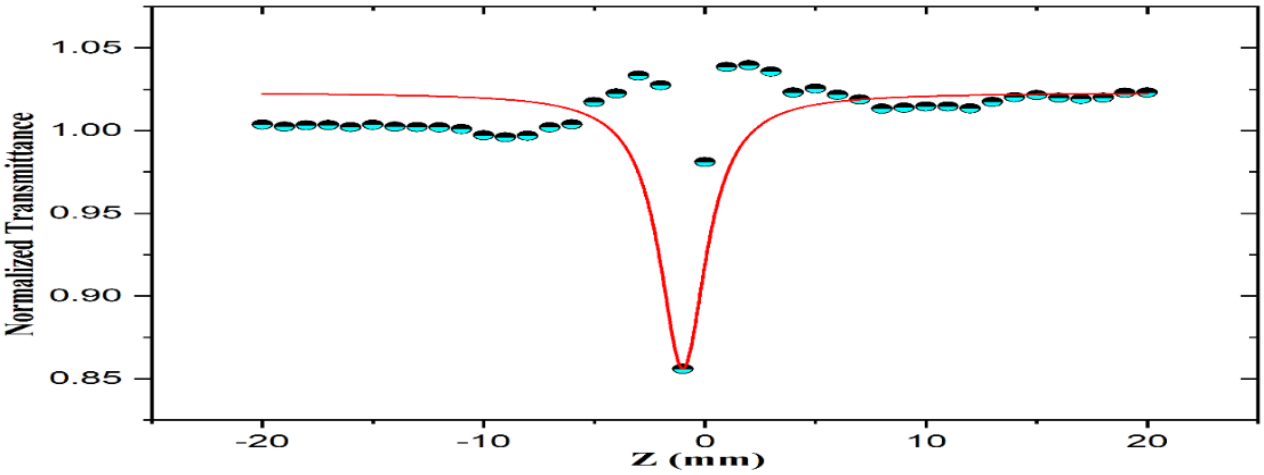

Figure 5.7.1 Open aperture z-scan of (2E)-2-(3,4-Dimethoxybenzylidene)-3,4-dihydronaphthalen-1(2H)-one under continuous wave mode

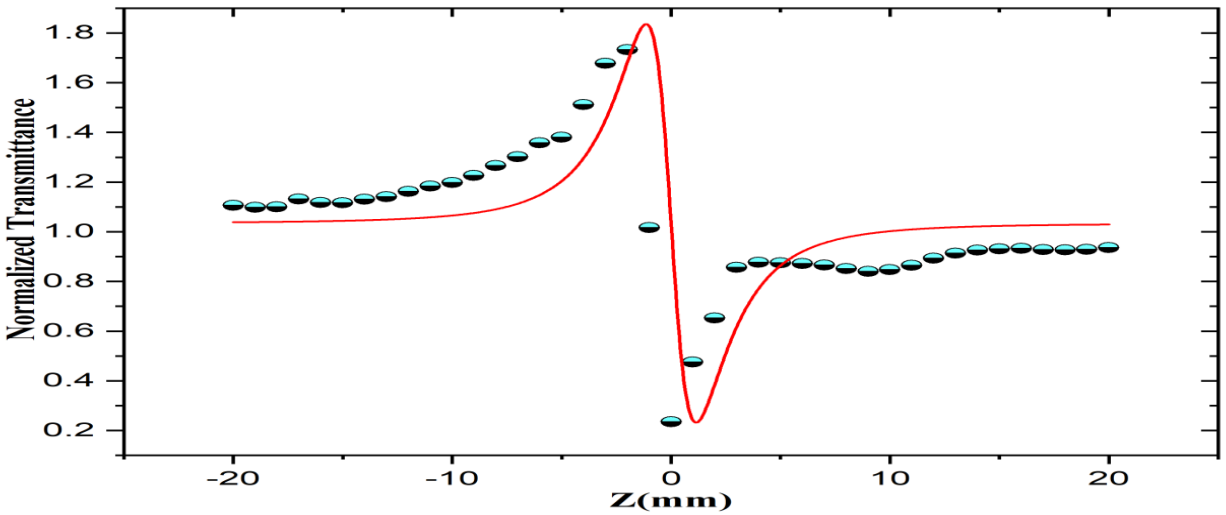

Figure 5.7.2 Closed aperture z-scan of (2E)-2-(3,4-Dimethoxybenzylidene)-3,4-dihydronaphthalen-1(2H)-one under continuous wave mode

The precisely noted pre-focal peak and post-focal valley signature in the closed aperture z-scan proclaim a negative nonlinearity (self de-focusing property) under continuous wave (CW) excitation. This nonlinearity points to potential optical limiting application of the crystal in the CW regime. The nonlinear optical parameters including the linear refractive index (n_0), third order refractive index (n_2), nonlinear absorption coefficient (β) and third order susceptibility (χ^3) obtained from the study are given in **Table 5.7.1.**

Table 5.7.1. Nonlinear optical parameters of (2E)-2-(3,4-Dimethoxybenzylidene)-3,4-dihydronaphthalen-1(2H)-one obtained from continuous wave z-scan.

n_0	1.0249
n_2 (cm^2/W)	3.30×10^{-09}
β (cm/W)	2.72×10^{-04}
Re $\chi(3)$ (esu)	4.21×10^{-06}
Im $\chi(3)$ (esu)	1.17×10^{-07}
$\chi(3)$ (esu)	4.21×10^{-06}

CHAPTER 6

CONCLUSION AND FUTURE SCOPE

6.1 CONCLUSIONS

The organic NLO crystal (2E)-2-(3,4-Dimethoxybenzylidene)-3,4-dihydronaphthalen-1(2H)-one has been synthesized by solvent evaporation method, its crystal structure is confirmed with the help of single crystal XRD analysis. The crystal structure has been optimized using the Gaussian 09 software at the B3LYP/cc-pVTZ level and linear regression analysis shows good agreement between the experimental and computed parameters. The potential nonlinearity of the title compound is manifested from the strong electron delocalization, intramolecular hydrogen bonding,and charge transfer interaction within the molecule, which are evident from the NBO analysis. The NBO analysis also reveals the hyper conjugative interactions ICT and the stabilization of molecules. The UV-visible spectral analysis of the title compound in acetone gives a strong transition at 349 nm which is due to the $n \rightarrow \pi^*$ transition and a high transmittance percentage in the entire visible region (380–800 nm) makes it a good candidate for NLO applications. The narrow HOMO-LUMO energy gap which is 2.1146 eV denotes a soft compound. Vibrational assignments were performed at B3LYP/cc-PVTZ level of theory, and the experimental and simulated IR spectra were compared. The electronic contributions to the polarizability and hyperpolarizabilities of the title compound with their static and frequency dependent characters have been studied theoretically and are found to be superior to those of urea. The third order nonlinearity of the title compound measured from the z-scan studies in continuous wave excitation regime, confirms its substantial optical nonlinearity which points to its potential optical limiting applications.

6.2 FUTURE SCOPE

Chalcone derivatives have long been used in nonlinear optics due to the fact they permit the modification of the substituents connected to the aromatic ring and the consequent changes in the optical properties of the material. These properties are reflectance of the significant delocalization of

the π electrons of the molecular system. The applications of these materials are found in information carrying, data storage, telecommunications, lasers, optical sensing, optical computers and in designing optical systems and components. Beyond these applications, chalcones are renown for the biological applications also. As an emerging area of research, the synthesis of new organic crystals and the study of their nonlinear properties have many importance. Further studies on this can make many devices easily available to all in affordable prices, as organic material derivatives can be easily made.

In this work, a novel chalcone derivative was synthesised and the theoretical and experimental studies on the structure, electronic and vibrational spectral studies of the compound was done. Further studies on the title compound can be done to get to know more about its properties and applications. Raman spectra can be plotted and can be compared with that of IR, which can give information on the molecular symmetry according to mutual exclusion principle.

REFERENCES

[1] ***Zheng, S.M. Jiang, Z. Chen, B. J. Ye and H. Piao,"*** Synthesis and Anti-Bacterial Activity ***C*** of Some Heterocyclic Chalcone Derivatives Bearing Thiofuran, Furan, and Quinoline Moieties ***",*** *Arch. Pharm*., vol. 344, 2011**.**

[2] ***S. Chandran, Srinivasan Manikam, "***Optical Properties of Single Crystals***",*** DOI:10.5772/intechopen.95607,2021

[3] ***Shivaraj R. Maidur, Jitendra R. Jahagirdar, Parutagouda Shankaragouda Patil, Tze Shyang Chia, Ching Kheng Quah, "***Structural Characterizations, Hirshfeld Surface Analyses, and Third Order Nonlinear Optical Properties of Two Novel Chalcone Derivatives",*Elsevier*,2017

[4] ***R. B. T. C. Ralph, "***Better Computing with Photons", *Science*,2007

[5] ***B. Bransden***, Quantum Mechanics, 2000.

[6] ***B. Bransden,*** Physics of atoms and molecules, 1983.

[7] ***R. Resnick,*** Quantum Physics of Atoms, Molecules, Solids, Nuclei, and Particles, 1974**.**

[8] ***D. S. Sholl and J. A. Steckel***, Density Functional Theory: A Practical Introduction, 2009.

[9] ***F. Jensen,*** Introduction to Computational Chemistry, 1998.

[10] ***J. Burdett, M.-H. Whangbo and T. A. Albright,*** Orbital Interactions in Chemistry, 2013.

[11] ***E. G. Lewars***, Computational Chemistry: Introduction to the Theory and Applications of Molecular and Quantum Mechanics, *Springer*, 2003.

[12] ***H. Bernhard Schlegel***, Geometry optimization, *John Wiley & Sons, Ltd.*, Vol:1, Sept/Oct 2011.

[13] ***F. Weinhold and C. R. Landis,*** VALENCY AND BONDING-A Natural Bond Orbital Donor–Acceptor Perspective, *Cambridge University Press*, 2005**.**

[14] ***F. Weinhold, C. Landis and E. Glendening,*** "What is NBO analysis and how is it useful?", *International Reviews in Physical Chemistry*, vol. 35, no. 3, 2016**.**

[15] ***A. E. Reed, L. A. Curtiss and F. Weinhold***, "Intermolecular interactions from a natural bond orbital, donor-acceptor viewpoint," *Chemical Reviews*, vol. 88, no. 6, 1988.

[16] ***F. Weinhold***, "Natural bond orbital analysis: A critical overview of relationships to alternative bonding perspectives," *Journal of computational chemistry*, vol. 33, no. 30, 2012.

[17] E. D. Glendening, C. R. Landis and F. Weinhold, "Natural bond orbital methods**,"** *Wiley interdisciplinary reviews: computational molecular science*, vol. 2, no. 1, 2012.

[18] ***C. N. Banwell and E. M. McCash***, Fundamentals of molecular spectroscopy, *McGraw- Hill*, 1972

[19] ***R. Kakkar***, Atomic and Molecular Spectroscopy, *Cambridge University Press*, 2015.

[20] ***Eric W. Van Stryland, Mansoor Sheik-Bahae,***" Z-Scan Measurements of Optical Nonlinearities", Characterization Techniques and Tabulations for Organic Nonlinear Materials, M. G. Kuzyk and C. W. Dirk, Eds., page 655-692, Marcel Dekker, Inc.,1998

[21] ***M. Karelson, V. S. Lobanov and A. R. Katritzky***, "Quantum-Chemical Descriptors in QSAR/QSPR Studies," *Chemical Reviews*, vol. 96, no. 3, 1996.

[22] ***P. Thanikaivelan, V. Subramanian, J. R. Rao and B. U. Nair***, "Application of quantum chemical descriptor in quantitative structure activity and structure property relationship," *Chemical Physics Letters*, vol. 323, no. 1-2, 2000.

[23] ***N Balamurugan, A. Arulchakkaravarthi, S. Selvakumar, M. Lenin, Rakesh Kumar, S. Muralithar, K. Sivaji, P. Ramasamy***, "Growth and characterization of undoped and Thallium doped CsI single crystals".

[24] ***Bunaciu AA, Udriştioiu EG, Aboul-Enein HY***. "X-ray diffraction: instrumentation and applications", *Crit Rev Anal Chem*. 2015;45(4):289-99. doi: 10.1080/10408347.2014.949616. PMID: 25831472.

[25] ***Lynnette Joseph, D. Sajan, Venkataraya Shettigar, K. Chaitanya, Neeraj Misra, Tom Sundius, I. Nemec***, "Synthesis, crystal growth, thermal studies and scaled quantum chemical studies of structural and vibrational spectra of the highly efficient organic NLO crystal: 1-(4-Aminophenyl) -(3,4-dimethoxyphenyl)-prop-2-en-1-one"

[26] ***M. Zarraga, F. Rivera, P. Arroyo, A. Miranda, R . Baggio, L. Alvares and Y. Moreno***, "Synthesis and crystal structure analysis of a new chalcone derivative of apocynin", Journal of Chilean Chemical Society, vol. 65 No 3(2020)

[27] ***V. S. Naik, H. S. Jayanna and G. Vinitha***, "Synthesis, molecule growth, characterization, theoretical studies and nonlinear optical properties of new chalcone derivative containing thiophene moiety for optical device applications.," *Indian Journal of Physics (July2020)*

[28] ***V. S. Naik, P. S. Patil, N. B. Gummagol, Q. A. Wong, C. K. Quah and H. Jayanna***, "Crystal structure, linear and nonlinear optical properties of three thiophenyl chalcone derivatives: A combined experimental and computational study.," *Optical Materials*, vol. 110 ,2020

[29] ***M. P. S. Yadav, A. Kumar and A. Jayarama,*** "Vibrational spectra analysis, NBO, HOMO–LUMO, and nonlinear optical behaviour studies on 3-(3, 4-dimethoxyphenyl)-1-(pyridin-2-yl) prop-2-en-1-one.," *Monatshefte für Chemie-Chemical Monthly* , vol. 147, no. 6, 2016.

[30] ***S. Sebastian and N. Sundaraganesan***, "The spectroscopic (FT-IR, FT-IR gas phase, FT-Raman and UV) and NBO analysis of 4-Hydroxypiperidine by density functional method.," *Spectrochimica Acta Part A: Molecular and Biomolecular Spectroscopy*, vol. 75, no. 3, 2010.

[31] ***P. V. Sreelaja and C. Ravikumar***, "Structural and vibrational spectral contributions to the nonlinear optical properties of 2-Amino-3-nitropyridinium 4-hydroxybenzenesulfonate: A DFT study", *Journal of molecular structure*, vol.1223(5^{th} jan.2021)

[32] ***A. Kumar, V. Deval, P. Tandon, A. Gupta and E. D. D'silva,*** "Experimental and theoretical (FT-IR, FT-Raman, UV–vis, NMR) spectroscopic analysis and first order hyperpolarizability studies of non-linear optical material:(2E)-3-[4-(methylsulfanyl) phenyl]-1-(4-nitrophenyl) prop-2-en-1-one using density functional theory," *Spectrochimica Acta Part A: Molecular and Biomolecular Spectroscopy*, vol. 130 , 2014.

[33] ***Tongpeng Zhao, Chunmei Wang, Siyuan Hu, Shaohua Ji, Chen Hu,Kai Xu, Bing Teng***," Structural design and characterization of a chalcone derivative crystal DAMO with strong SHG efficiency for NLO applications", *Optical Materials*, vol.112,February 2021**.**

[34] ***Kai Xu,Rui Chen, Jinkang Ma, Tianghua Wang, Degao Zhong, Lifeng Cao, Bing Teng and Haitao Wu****," "* Molecular Structure Design, Crystal Growth, and Characterization of New Types of Organic Nonlinear Optical Chalcone Crystals*",* ***Crystal Growth and Design,*** June 1,2022.

[35] ***Leonardo R. Almeida, Murilo M. Anjos, Gabriela C. Ribeiro, Clodoalo Valverde, Daniel F. S. Machado, Guilherme R. Oliviera, Hamilton B. Napolitano and Heibbe C. de Oliveira,*** *"Synthesis, structural characterization and computational study of a novel amino chalcone: a potential nonlinear optical material****",*** *New Journal of Chemistry*, issue 4,2017

[36] ***J. Christina Jebapriya, D. R Jonathan, S. R. Maidur, P. Nallamuthu, P. S. Patil, J. C. Prasana***, "Crystal structure, synthesis, growth and characterization of a non-linear chalcone crystal(2E)-1-(4-chlorophenyl)-3-(4-diethylaminophenyl)-prop-2-en-1-one", *Journel of Molecular Structure*,vol.1246, December 2021.

[37] ***V. M. Bhumannavar, P. S. Patil, N. B. Gummagol,*** "Structure characterization, spectroscopic investigation and nonlinear study using Density Functional Theory of (E)-1-(4-Chlorophenyl)-3-(4-methylphenyl) prop-2-en-1-one", *AJRC*,vol.15, issue.2,2022

[38] ***Nurul Husna Norwawi, Siti Nor Fatihah Johari, Siti Nabilla Aliya Mohd Nizar, Siti Noor Farhana Ab Rahman, Ainizatul Husna Anizaim, Ibrahim Abdul Razak, Suhana Arshad***, "Synthesis, structural investigation and computational analysis on a new chalcone derivative: (E)-1-(benzo[d][1,3]dioxol-5-yl)-3-(2-chloro-6-fluorophenyl)prop-2-en-1-one", *Chemical Data Collections*, Volume 38, 2022.

[39] ***Elizabeth Mathew, Vinutha V. Salian, B. Narayana, I. Hubert Joe***, "Experimental and Theoretical approach on third- order optical non-linearity of a highly efficient anthracene-based chalcone derivative for optical power limiting", *Journal of Molecular Structure*, Vol. 1250, Part 2,15, Feb.2022.

[40] Shirmila, D. A., Jonathan, D. R., Priya, M. K., Hemalatha, J., & Usha, G. (2021). (2E)-2-(3, 4-Dimethoxybenzylidene)-3, 4-dihydronaphthalen-1 (2H)-one. IUCrData, 6(3), x210309.

[41] ***Reed, A. E.; Curtiss, L. A.; Weinhold, F***. "Intermolecular Interactions from a Natural Bond Orbital, Donor-Acceptor Viewpoint". *Chemical Reviews* 1988, 88, 899–926. DOI: 10.1021/cr00088a005.

[42] ***Malar, C. T., Malar, S. P., & Kumaresan, P***. Analysis Of Frontier Molecular Orbitals And Molecular Electrostatic Potential Of Methyl Red Doped L-Arginine Phosphate Crystals For Laser Applications.

[43] ***Meganathan, C., Sebastian, S., Kurt, M., Lee, K. W., & Sundaraganesan, N***. "Molecular structure, spectroscopic (FTIR, FTIR gas phase, FT-Raman) first-order hyperpolarizability and HOMO–LUMO analysis of 4-methoxy-2-methyl benzoic acid", *Journal of Raman Spectroscopy*, *41*(10), 1369-1378, (2010).

[44] ***Kumari, M. M., Indu Ramachandra, M. P., Ravikumar, C., Joe, I. H., & Němec, I.*** "Charge transfer interaction and nonlinear optical properties of barium chloride and thiourea complexes: a vibrational spectroscopic study". *Journal of Raman Spectroscopy*, *42*(6), 1462-1469. (2011).

[45] ***Sreelaja, P. V., & Ravikumar, C***. "Charge transfer interaction and vibrational spectral investigation of 2-amino-5-nitropyridinium sulfamate". *Spectroscopy Letters*, *52*(9), 492-509. (2019).

[46] ***Socrates, G, "***Infrared characteristic group frequencies, Tables and charts". *Journal of the American Chemical Society*, *117*(5), 1671-1671, (1995)

[47] ***Sajan, D., Joe, I. H., & Jayakumar, V. S,*** "NIR-FT Raman, FT-IR and surface-enhanced Raman scattering spectra of organic nonlinear optic material: p-hydroxy acetophenone". *Journal of Raman Spectroscopy: An International Journal for Original Work in all Aspects of Raman Spectroscopy, Including Higher Order Processes, and also Brillouin and Rayleigh Scattering*, *37*(4), 508-519, (2006).

[48] ***Varsányi, G.*** Assignments for vibrational spectra of seven hundred benzene derivatives (Vol. 1). *John Wiley & Sons*., (1974).

[49] ***Colthup, N***. Introduction to infrared and Raman spectroscopy. *Elsevier*. (2012).

[50] ***Gussoni, M., & Castiglioni, C***. "Infrared intensities. Use of the CH-stretching band intensity as a tool for evaluating the acidity of hydrogen atoms in hydrocarbons", *Journal of Molecular Structure*, *521*(1-3), 1-18, (2000).